港湾技研資料

TECHNICAL NOTE OF
THE PORT AND HARBOUR RESEARCH INSTITUTE
MINISTRY OF TRANSPORT, JAPAN

No. 787 Dec. 1994

OPERATION OF PHRI GEOTECHNICAL CENTRIFUGE FROM 1980 TO 1994

遠心模型実験装置の運転の記録（1980年～1994年）

北　詰　昌　樹
寺　師　昌　明

運輸省港湾技術研究所

Operation of PHRI Geotechnical Centrifuge from 1980 to 1994

CONTENTS

Synopsis 3

1. Introduction 3

2. Development of the PHRI Mark I Centrifuge 4

2.1 General Arrangements of the Centrifuge 4

2.2 Ancillary Equipment 8

2.3 Machine Use 10

2.4 Safety 11

3. Research Subjects Studied 12

3.1 Bearing Capacity of Sand Ground 12

3.2 Bearing Capacity of Clay Ground 18

3.3 Behavior of Fabric-Reinforced Clay Ground under Embankment 20

3.4 Bearing Capacity of Improved Ground by Sand Compaction Piles 24

3.5 Horizontal Resistance of a Pile in Sand 27

3.6 Consolidation Behavior of Soft Clay with Fabri-Packed Sand Drain 30

3.7 External Stability of Improved Ground by Deep Mixing Method 32

4. Concluding Remarks 35

References 36

List of symbols 43

遠心模型実験装置の運転の記録(1980年～1994年)

北　詰　昌　樹*
寺　師　昌　明**

要　旨

当所では，1980年に有効半径3.8m，最大加速度115gの世界最大級の遠心模型実験装置（Mark Ⅰ）を導入して以来，これまで1300回を超える模型実験を実施してきた。しかし，装置の老朽化と新しい研究テーマに対応するため，1989年より新遠心模型実験装置（MarkⅡ）の建設を進めている。1994年の新遠心装置の完成に際して，現有の装置は解体され，その役目を終えた。

本稿では，遠心装置ならびに周辺機器の紹介と，14年にわたる研究成果を簡単に紹介し，遠心模型実験手法の有用性を示した。

*　土質部地盤改良研究室長
**　㈱日建設計中瀬土質研究所副所長
（前土質部地盤改良研究室長）

Operation of PHRI Geotechnical Centrifuge from 1980 to 1994

Masaki KITAZUME*
Masaaki TERASHI**

Synopsis

In 1980, the Port and Harbour Research Institute (PHRI) constructed a centrifuge (Mark I) of 3.8m effective radius. Since then PHRI Geotechnical Group has conducted more than 1300 centrifuge operations and has published nearly 60 papers related to centrifuge model tests.

In 1989, PHRI has started the construction of a new facility to house Mark II centrifuge adjucent to the existing centrifuge facility. In April of 1994 when the Mark II centrifuge was assembled in site, the Mark I centrifuge was disassembled. Many research projects related to centrifuge model testing will also be performed by the Mark II centrifuge.

This paper briefly describes the developments of the PHRI Mark I centrifuge facilities and centrifuge operations experienced in the past 14 years. Research subjects studied so far are reviewed to demonstrate usefulness of this modeling technique and ability of our centrifuge facilities.

KEY WORDS: Test Equipment, Centrifuge Model Test

*Chief of Soil Stabilization Laboratory, Geotechnical Division
**Deputy Director, NIKKEN SEKKEI Nakase Geotechnical Institute, former Chief of Soil Stabilization Laboratory

1. Introduction

In geotechnical engineering, small-scale model tests are sometimes used to study the complex nature of soil response and soil-structure interaction. However, it is known that soil response depends on the level of effective stress within the soil mass. Therefore, small-scale model tests in a conventional gravity field of $1g$ often fail to reveal some important phenomena that may exist at the prototype stress level.

To overcome this situation, it is desirable to perform a small-scale test at field stress level conditions. One method of doing this is the centrifuge technique, in which a small model scaled $1/n$ from the assumed prototype is tested under an "n" times gravity field created by the centrifugal acceleration. Principle of geotechnical centrifuge modeling has been appreciated since the 1930s and explained by several research workers[1]. At present, centrifuge testing has become an important tool for the investigation of complex geotechnical nature as referenced by several recent symposia.

Currently more than five dozens geotechnical centrifuges are in operation in various countries. In Japan Prof. Mikasa at Osaka City University was the first who built a centrifuge of 1.01 m effective radius in 1965 and utilized it to study the consolidation process of soft clay. In the 1960s, the Tokyo Institute Technology built a centrifuge of 1.18 m effective radius. These two centrifuges were much utilized to investigate the self weight consolidation, bearing capacity of soil and so on. These research efforts and achievements proved the importance of centrifuge model testing.

In 1980, the Port and Harbour Research Institute (PHRI) constructed a centrifuge of 3.8 m effective radius. For prototype structure in port and harbor area, a reasonable soil area to be modeled was considered to be 150 m * 150 m in plane. Therefore the effective radius, maximum acceleration and space of the swinging platform of the PHRI centrifuge were determined as around 3.5 m, 100 g and 1.5 m * 1.5 m, respectively. This provided many research engineers in Japan with motivation to build up their own centrifuges.

Since then PHRI has conducted more than 1300 centrifuge operations and has published nearly 60 papers related to centrifuge model tests. Some of research projects were conducted with close relation to specific prototypes, and research results have been reflected to the actual constructions.

Since 1989, undesirable vibrations of the concrete pit floor have frequently occurred during high speed operation. This phenomenon was due to the progress of cracks in the concrete pit floor. After detailed investigation, maximum operative acceleration was reduced below 50 g for safety reasons. And PHRI also decided to construct a new centrifuge, Mark II. In 1989, PHRI has started the construction of a new facility to house Mark II centrifuge adjacent to the existing centrifuge facility. During six years construction period of the Mark II Centrifuge, Mark I centrifuge had been operated as usual below the limited acceleration. Drive system, control system and data acquisition system are totally replaced by the advanced systems for Mark II. The beam and swinging platform of the Mark I were took over to the Mark II centrifuge. In April of 1994 the Mark I was disassembled and the Mark II was installed. Many research projects related to centrifuge model testing will also be performed in the Mark II centrifuge.

This paper briefly describes the developments of the PHRI Mark I centrifuge facilities and centrifuge operations experienced in 14 years. Research subjects studied so far are reviewed to demonstrate usefulness of this modeling technique and ability of our centrifuge facilities.

2. Development of the PHRI Mark I Centrifuge

2.1 General Arrangements of the Centrifuge

The construction of the PHRI Mark I Centrifuge began in 1977 and completed in March of 1980. The basic machine configuration and assembly have been described by Terashi[2),3)] and are only briefly described here, together with the development of associated hardwares.

The main part of the centrifuge is housed in the underground reinforced concrete pit for safety operation as shown in Figs. 1 and 2. The inner size of the pit is 10.4 m in diameter and 4.2 m in height. As the soft rock appeared at the depth of 3.5 m at the site, the bottom of the pit was buried in the soft rock. Main part of the centrifuge weighs approximately 87 tons and whose diameter is 9.5 m. Two swinging platforms are hinged to the rotating arm via the torsion bar systems to safely deliver the radial force at high acceleration to the end plates at both ends of the arm.

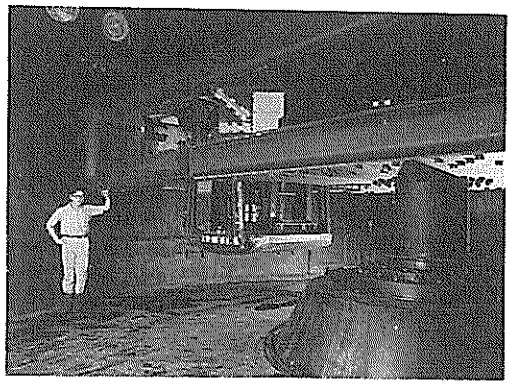

Fig.1 Photograph of PHRI Centrifuge

The drive unit for the centrifuge of 400 kW direct current motor is mounted on the upper floor of the pit and generates steady acceleration up to 115 g at the surface of the swinging platform whose radius during flight is 3.8 m. Major specifications of the PHRI centrifuge are listed in the Table 1. The control of the centrifuge is conducted in the operation room. Conditions of all the important components of the centrifuge, such as radial and thrust bearing of the main shaft, electric currents, air conditioner, lubrication, and etc. are always monitored and displayed on the control panel. Safety functions are equipped to ring the alarm in the case of trivial troubles and to stop the machine automatically in the case of severe trouble.

Table 2 and figure 3 show the comparison of the capacity of major centrifuges available in the literature[1),2),4)-43)]. The PHRI centrifuge is still one of the major large centrifuge in the world.

2.2 Ancillary Equipment

Various tools and equipments to conduct experiments in a high g field are available, such as loading devices for bearing capacity study, sand hopper for embankment construction, vane tester and cone-penetrometer for measuring in-situ strength of the model ground. In order to drive these equipments during flight, rotary transformer is installed at the upper part of main shaft to supply electricity of 3ϕ 200V to the centrifuge. The electricity is transformed to 2ϕ 100V, DC 6-24V and each electricity can be controlled individually by means of switching circuit. Hydraulic pressures are also supplied to the platform through rotary hydraulic joints.

Electric signals obtained by various transducers are transmitted through a slip ring stack of 80 poles on the top of the main shaft from the swinging platform to the operation room. The analog signals from transducers are measured and converted to digital signals by a strain meter, inputted to a personal computer, stored in a cartridge tape and displayed on the CRT after some computation. The personal computer for the data acquisi-

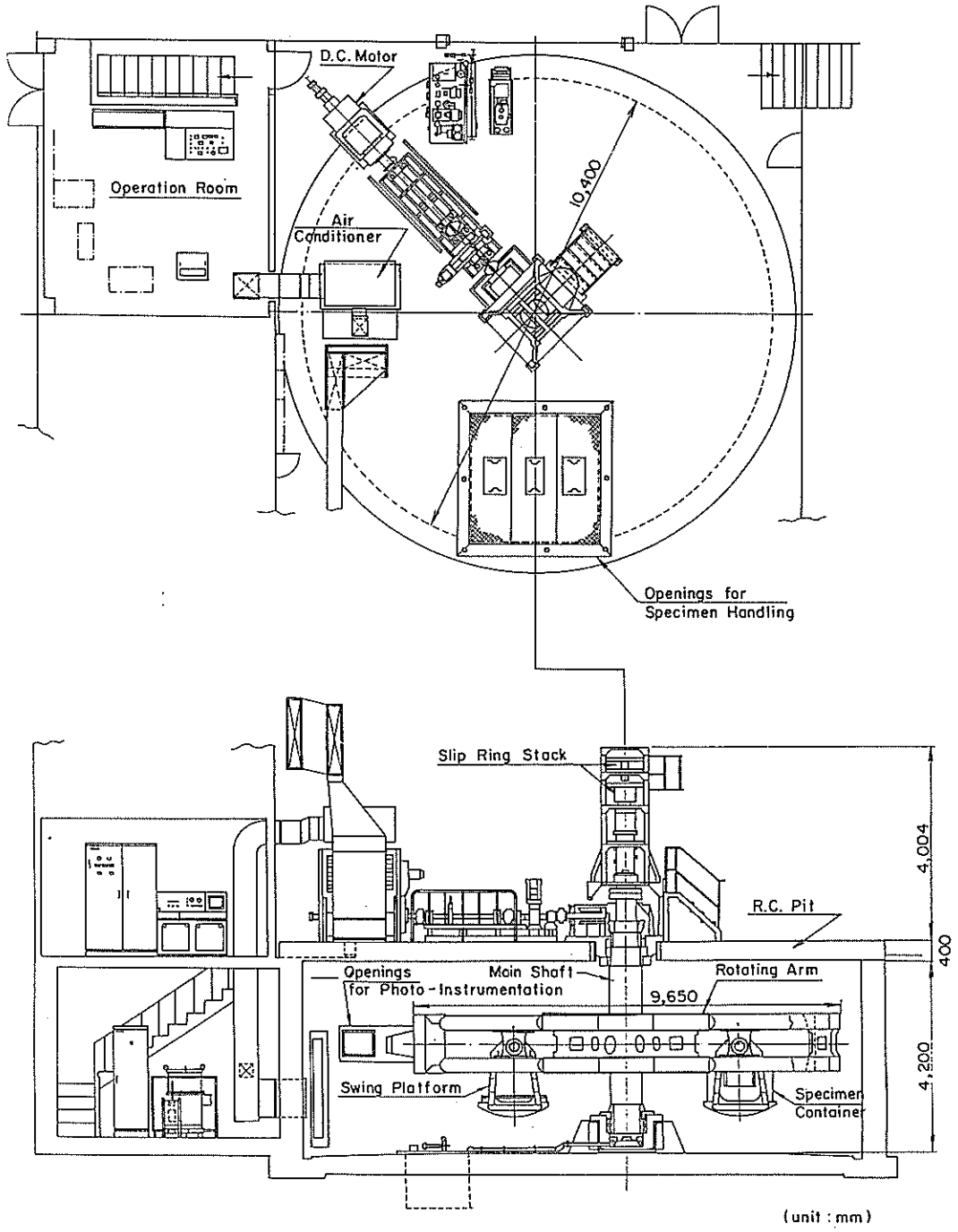

Fig.2 PHRI Centrifuge

Table 1 Major Specifications of PHRI Centrifuge

Maximum acceleration (g)	115
Diameter of rotating arm (mm)	9,650
Maximum effective radius (mm)	3,800
Maximum Number of rotation (rpm)	165
Space of swinging platform (mm)	1,600×1,600
Maximum payload (kg)	2,710
Maximum capacity (g-tons)	300
Main motor (kW)	400
Electric slip ring (poles)	80
Rotary transformer (kVA)	5.2
Number of hydraulic joints	10
Total weight of the centrifuge (tf)	87

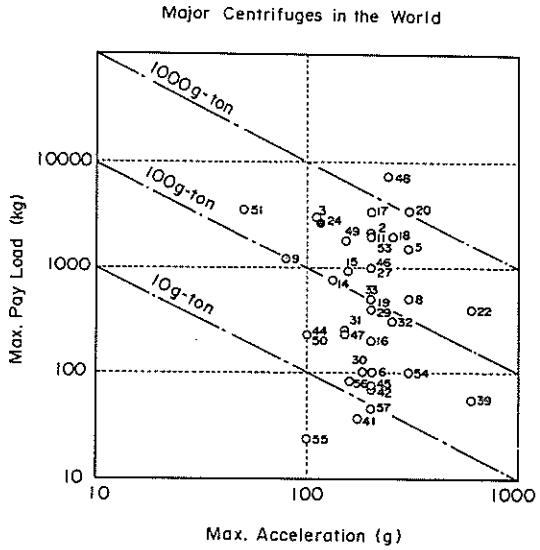

Fig.3 Comparison of Capacity

Table 2 Major Centrifuge in the World

No.	Institution	Country	Max. Radius (m)	Effective Radius (m)	Max. Accel. (g)	Max. Payload (kg)	Capacity (g-ton)
1	The University of Western Australia	Australia	1.8	1.55	200	400	40
2	C-CORE	Canada	5.5	5	200	2200	220
3	Chengdu Hydroelectric Investigation and Design Institute	China		10.8	110	3000	216
4	Hehai University	China		2.4	250		25
5	Institute of Water Conservancy and Hydroelectric Power Research	China	3		300	1500	450
6	Nanjing Hydraulic Research Institute	China	3	2	200	100	20
7	Nanjing Hydraulic Research Institute	China		5	200	2000	400
8	Yangtze River Science Research Institute	China	3.47	3	300	500	150
9	Danish Engineering Academy	Denmark		2.3	80	1200	96
10	CESTA	France	10				
11	LCPC	France	5.5	5	200	2000	200
12	City University	UK	1.8	1.55	200	400	40
13	Lucas Aerospace Division	UK	2.6				
14	UMIST	UK		1.5	133	750	100
15	University of Cambridge	UK	4.3	4	155	900	
16	University of Liverpool	UK		0.991	200	200	20
17	University of Manchester	UK	3.2		200	3400	
18	Ruhr-Univ.	Germany		4.125	250	2000	500
19	Ruhr-Univ.	Germany	1.8	1.55	200	400	40
20	Delft University of Technology	Holland			300	3500	
21	Israel Defence Ministry	Israel	1.5		100		
22	ISMES	Italia			600	400	
23	NIKKEN SEKKEI	Japan	3	2.7	200	1000	100
24	Port and Harbour Research Institute, Mark-1	Japan		3.8	115	2710	300
25	Kyoto University	Japan		1.5	200		
26	Ministry of Construction	Japan		1.15	300		
27	Kashima Co.	Japan	3	2.7	200	1000	100
28	Osaka City University, Mark-5	Japan		2.56	200		22.4
29	Taisei Co.	Japan		2.65	200	400	80
30	Chuo University	Japan	3.05		180	100	
31	Tokyo Institute Technology, Mark-2	Japan		1.25	150	250	37.5
32	Toyo Construction	Japan		2.2	250	300	75
33	Ministry of Labor	Japan	2.31		200	500	
34	Hydroproject Institute	Russia	2.5		320		
35	Institute of Ukr.N.I.I. Projekt	Russia		2.505	320		
36	Research Institute of Bases and Underground Structures	Russia	2		100		
37	VNII Vodgeo	Russia		2.3	250		
38	National University of Singapore	Singapore					
39	Boeing Aerospace Company	USA	1.4		600	55	66
40	Bureau of Mines at Maryland	USA	0.9				
41	California Institute of Technology	USA	1.3		175	36	7.5
42	MIT	USA			200	68	15
43	Missouri School of Mines at Rolla	USA	1.07				
44	New Mexico Engineering Research Institute	USA	1.8		100	227	25
45	Princeton University	USA	1.3		200	76	10
46	Rensselar Polytechnic Institute	USA	3	2.7	200	1000	100
47	Sandia Corporation : CA-2	USA	2.1		150	227	15
48	Sandia Corporation : fixed	USA	7.62		240	7257	800
49	Sandia Corporation : swing	USA	7.62		150	1814	300
50	US Air Force Engineering and Services Center	USA	1.83		100	225	15
51	University of California at Davis	USA		9.1	50	3640	275
52	University of California at Davis	USA	1		175		5
53	University of Colorado at Boulder	USA	5.49		200	2000	440
54	University of Colorado at Boulder	USA	1.36		300	100	15
55	University of Florida : A	USA	1		100	22.7	2.5
56	University of Florida : B	USA	2		160	83.9	
57	University of Maryland	USA	1.34		200	45.4	10

tion was originally HP-9825A (YHP) and replaced in 1988 by PC-9801 (NEC) for speedy acquisition. And the strain meter and switch boxes were also replaced by the more sophisticated ones, TDS-301 (Tokyo Sokki Co. LTD.), as shown in Fig.4. The signals to control the switching circuit are also transmitted through the slip ring from the operation room to the centrifuge.

Photograph of the model ground in the specimen box can be taken from two positions of the pit; the one is the opening at the side wall of the concrete pit, the shooting window I and the other is the opening at the upper floor of the pit, the shooting window II as shown in Fig.5. Two set of photographic systems were installed in 1980 at two shooting windows. Figure 6 shows the 70 mm pulse data camera installed at the shooting window I. The coordinates of the targets on a model taken during flight are digitized on a large screen (Fig.7) to real coordinate after compensation for various sources of distortion using fiducial points on the specimen box. To increase the quality of photographic image, every optical part of the system is specially designed[2),44)]. The data processor was originally HP-9825A (YHP) and replaced by PC-9801 (NEC) in 1988.

A TV monitoring system was also installed to the photographic system in 1980 at the shooting window I, which is quite powerful in real time observation and quick playback although the image quality is inferior to the still photograph. The same light source with that for still photograph is used for TV monitoring.

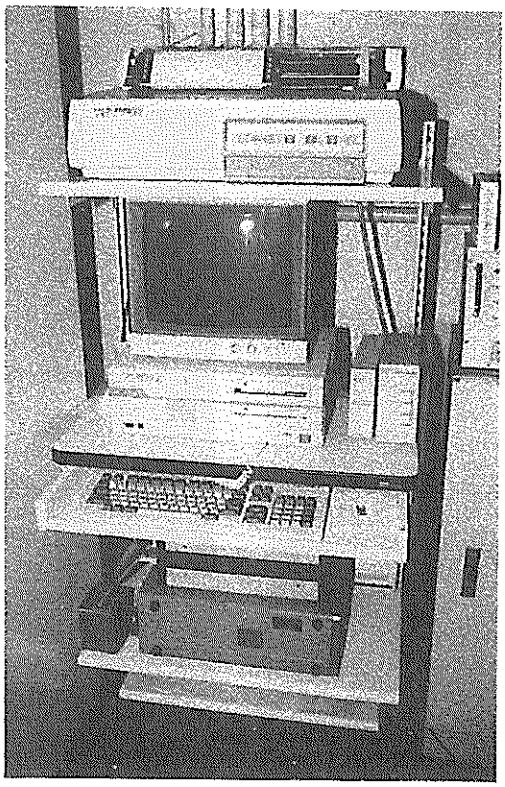

Fig.4 Data Acquisition System

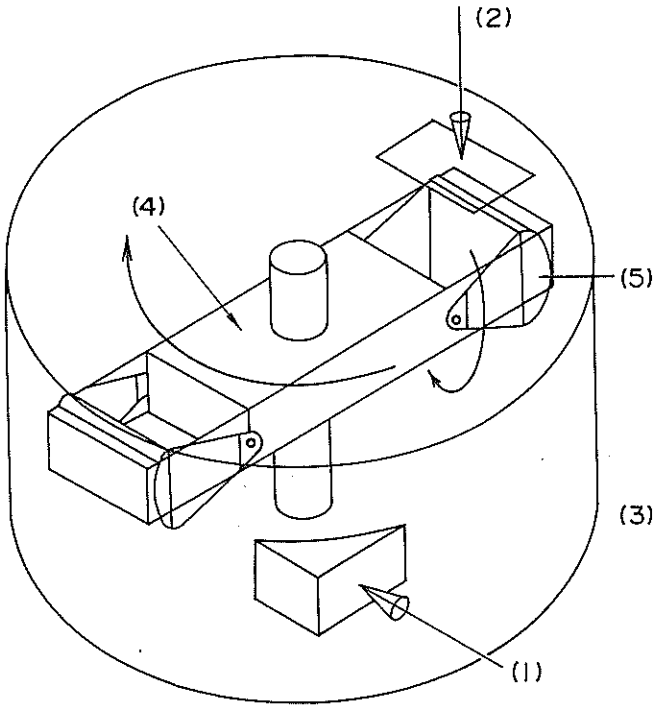

Fig.5 Schematic View of Centrifuge

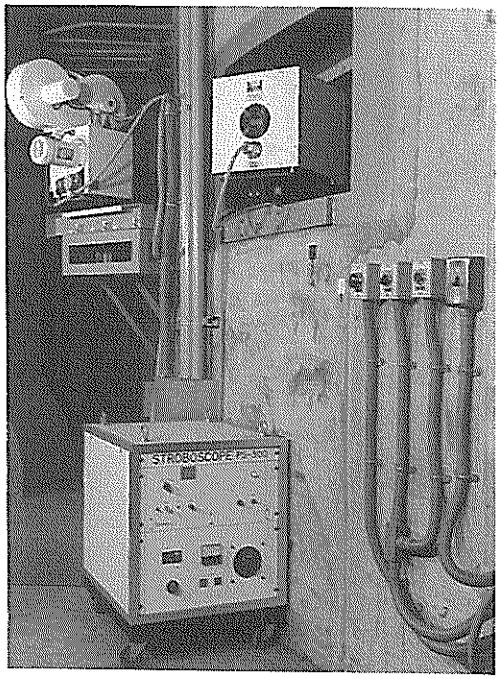

Fig.6 70 mm Pulse Data Camera at the Shooting Window I

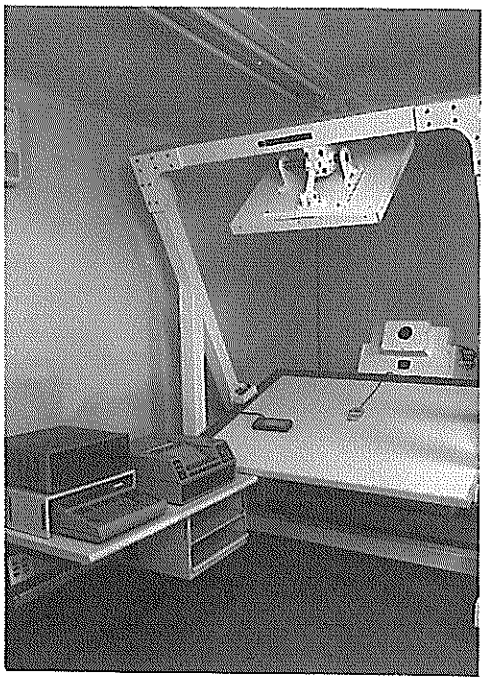

Fig.7 Projector, Digitizer and Data Processor

2.3 Machine Use

In the period 1980 to 1994 usage of the centrifuge can most conveniently be assessed in terms of number of machine runs, total running hours and total running machine rotation. Figure 8 shows analyses on a yearly basis with an average usage over an 14 years period of 93 runs totaling 229 hours per year. Of the total number of machine runs over this period some have yielded geotechnical data; the remainder fall into a nonproductive category including machine testing, instrument calibration, equipment proving, and tests which have been aborted for one reason or another.

Up to 1983 use of the centrifuge was mainly on bearing capacity of sand ground. Since this subject was a first model test for the PHRI centrifuge, fairly simple model tests, concentric loading tests were carried out at first. Know-how on operating the centrifuge, model preparation as well as model test procedure have been accumulated during a large number of repeated tests.

From 1984 the involvement with work on cohesive material required a long run centrifuge operation for obtaining normally consolidated clay ground having the shear strength increases with depth. The clay often used in the model was Kaolin clay whose coefficient of consolidation was relatively large so that consolidation time required for self weight consolidation in the centrifuge could be reduced to one and half days for a ground of 20 cm thickness. For safety operation almost all staffs including responsible engineer carefully monitored both the machine and model ground during the long run. Model turn round times for cohesive materials have been governed not only by consolidation periods but also by personnel exhaustion in the long run operation. Therefore the model tests on cohesive

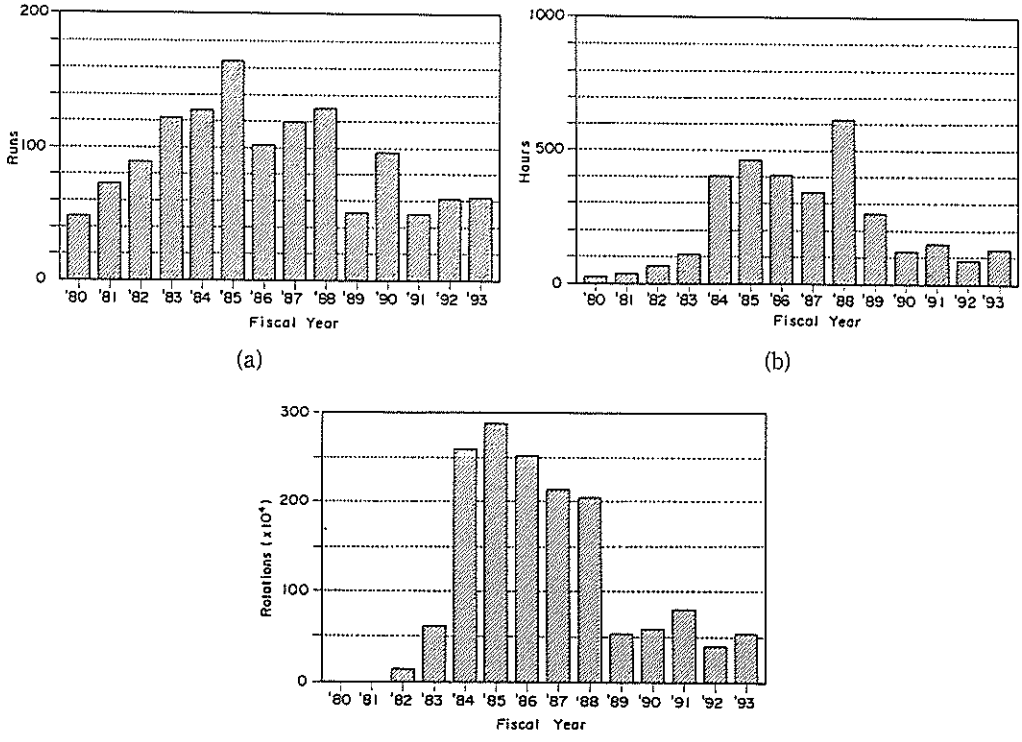

Fig.8 Annual Breakdown of Centrifuge Usage over an 14 Years Period

materials were carried out about once or twice a month and relatively short runs were carried out in the intervals of the long run operation.

Since 1989, undesirable vibration of the concrete pit floor has occurred at high speed running. This phenomenon was due to progress of fatigue cracks in the concrete pit. After detailed investigation and discussion with the manufacture, PHRI decided the maximum operative acceleration to be reduced below 50 g for short running and 40 g for long running for safety reasons.

2.4 Safety

An annual maintenance and a set of regulation contributed to the safe centrifuge operations for 14 years. The annual maintenance of about two weeks was undergone by the manufacturer to check the machine hardware, electric system, lubrication and so on. Since 1989, vibration of the concrete pit floor and the progress of the cracks in the pit were also checked during the annual maintenance.

The centrifuge was operated under a set of safety regulations, designed to minimize the risk of accidents to personnel or machinery. Model specimen boxes were designed by means of three dimensional elastic finite element analysis to ensure the stability and to confirm amount of expansion of the box during the flight within allowable value. All boxes thus designed and manufactured were subjected to proof testing in advance up to 20% higher acceleration than the acceleration of general use. In the proof test, the deformation, strains of various points of the box were measured and confirmed to remain within the allowable value. After these procedures, the boxes could be in use for model testing.

In model testing, every model and its counterweight were designed in advance on flight authorization sheets (Fig.9), to meet a balance requirement aimed at limiting wear on the machine bearings as a more stringent requirement than that of overall structural integrity. When model was mounted on the swinging platform of the centrifuge, all the equipment, transducers as well as loading devises were confirmed to suitably fixed in the presence of the responsible engineer.

During the centrifuge running a continuous check was done on the out-of-balance loads, temperature increase and noise in the rotary bearings, vibration of the machine and concrete pit floor.

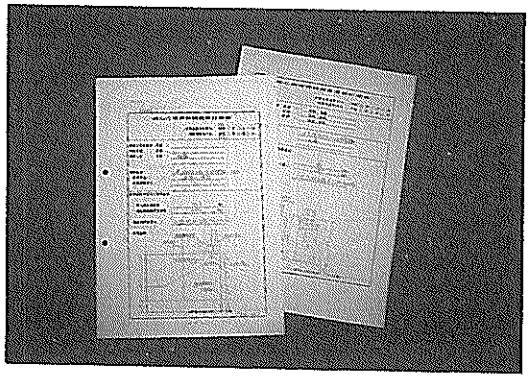

Fig.9 Flight Authorization Sheets

3. Research Subjects Studied

Figure 10 indicates area of research subjects over the 14 years. All projects have been assessed as project-orientated, curiosity orientated or both. As details of each subject have been presented elsewhere[45)-78)], test results of limited number of the subjects are briefly described here. In this article, units of pressure and force in the figures and tables of the original papers are converted into the SI units by a factor of 10 m/sec^2.

3.1 Bearing Capacity of Sand Ground[45)-49)]

The harbor area is almost always protected by breakwaters against incoming waves to keep the calmness of internal water and to maintain the required basin depth. In most cases in Japan, an upright breakwater of composite type is preferred which is usually composed of concrete caisson and rubble mound. Breakwaters also function to reduce the energy of earthquake-originated TSUNAMIs which have often attacked the coast lines of northern Japan. The breakwaters subjected to large horizontal force and moment raise a new problem to be solved.

As this research subject was a first one for our centrifuge, fairly simple model tests, concentric loading tests, were conducted at first to investigate the scale effect of the footing width on the bearing capacity as well as to accumulate the model test techniques.

(1) concentric loading test

The sand used is fine grained uniform Toyoura sand having uniformity coefficient, Uc of 1.38 and the effective grain size, D_{10} of 0.13 mm. The model ground of air dried Toyoura sand is prepared in the strong box on a laboratory floor by means of the multiple sieve method of sand raining to obtain uniform and density controlled sand ground throughout the test series. The average relative density of the sand is 95±5 %. The top surface of the ground is carefully leveled by sucking sand particles by a vacuum cleaner.

Results of concentric loading tests are shown in Fig.11. In the figure, the abscissa represents the generalized footing width γBn in which γ, B and n are unit weight of the sand ground, footing width and acceleration gravity respectively. The ordinate represents the bearing capacity factor $N\gamma$. In the experiments the actual model footing width was varied to 0.5, 1, 2, 3 or 4cm under various acceleration to obtain wide variety of generalized footing width. As shown in Fig.11 $N\gamma$ for the same γBn is almost same irrespective of the actual footing width. The scale effect on the bearing capacity can be clearly observed in which the bearing capacity decreases with the increase of generalized footing width. This phenomenon was also found by field and laboratory tests[79)] and centrifuge model tests[80)].

(2) eccentric loading test

A series of eccentric loading tests was performed in the condition of $\gamma Bn = 0.36$ to avoid the scale effect. This test series were also carried out on the dense Toyoura sand (Dr=95±5%). The reduction ratio of bearing capacity, $E\gamma$ is defined as a ratio of the eccentric bearing capacity against the concentric bearing capacity. The reduction ratio, $E\gamma$ with the increase in eccentricity is shown in Fig.12 together with available test data by various researchers[81)-84)]. The reduction ratio $E\gamma$ proposed by Meyerhof[81)] is also shown in the figure. Based on the experimental and analytical considerations on the condition of the loading point[45)], two kinds of loading tests, R and F loadings were performed. Although the test data has relatively large scatter, the centrifuge test results are fairly coincident with the other test data and the Meyerfoh's equation shows conservative value compared

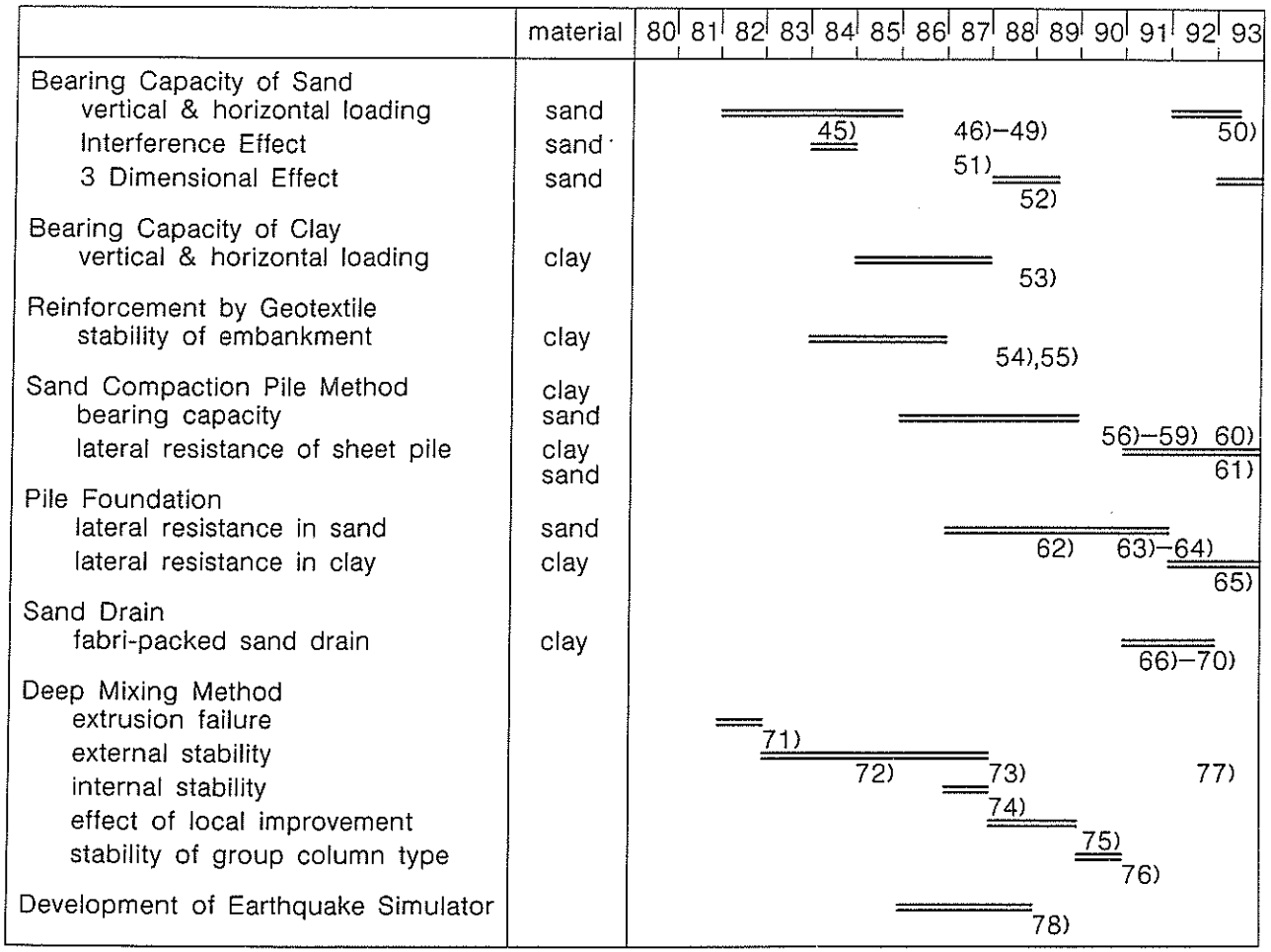

Fig.10 A Chronology of Research Subjects by the Use of Centrifuge

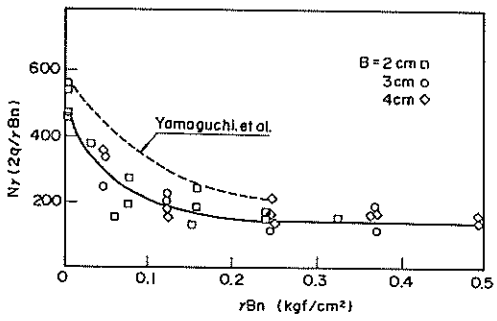

Fig.11 Nγ - γBn

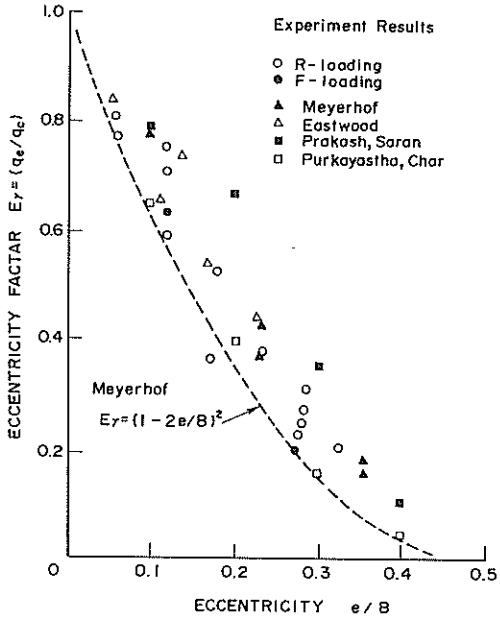

Fig.12 Eγ - e/B

with the test results.

(3) eccentric and inclined loading test

Under the action of eccentric vertical load, the rupture surface becomes one-sided. However there is a contradiction in the test results between most of past workers and Jumikis[85] regarding the direction of the rupture surface. By a series of centrifuge tests and elasto-plastic FEM analyses[15], it was concluded that the contradiction was due to the unexpected development of horizontal force at the loading point which was a consequence of the restriction to the free movement of the footing. Therefore to investigate the bearing capacity and rupture behavior a new loading devise was devised as shown in Fig.13 where the vertical and horizontal forces acting on the foundation could be individually controlled.

a) test procedure

After reaching the prescribed acceleration, the position of the foundation was adjusted exactly to the center line of the mound. The vertical load with a certain eccentricity was given by an air-cylinder and the foundation loads on the top surface of the mound. Then, finally, horizontal load was applied to the foundation and increased to failure of the mound at a constant displacement rate. To avoid the excessive change of eccentricity during the experiment, the air-cylinder was also pulled by the wire at the same horizontal displacement rate as that of the foundation. During the experiment, vertical load at the loading point, tension in the wire, vertical displacement of the loading point, and horizontal displacement of the foundation were measured directly by various transducers.

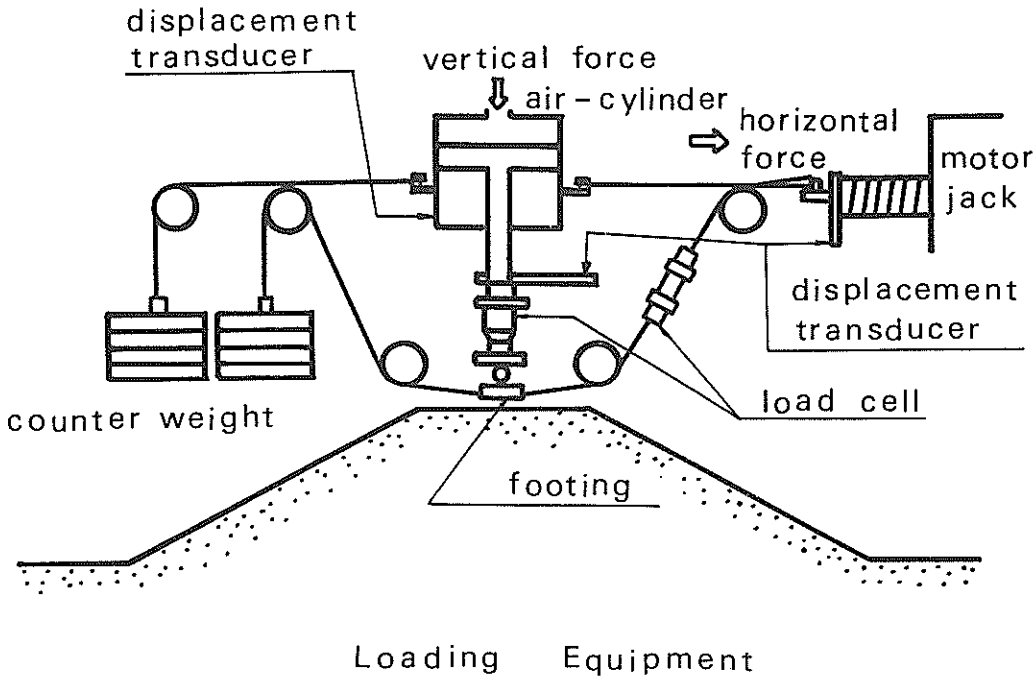

Fig.13 Loading Equipment

b) Horizontal load intensity - displacement relation

Relationships between the horizontal load component (H) and the horizontal displacement of the foundation (δ_h) are influenced by the applied vertical load level as shown in Fig.14. The H and δ_h curve for a lower vertical load level, as shown by open circles, has no peak. However, the curve for a higher vertical load level, as shown by open triangles, has a sharp peak at small displacement and shows a sudden reduction of resistance. The vertical load level for the curve shown by solid circles is between those for the above two curves and corresponds approximately to one half of the maximum vertical load sustained by the present mound.

c) Failure envelope in V-H-M space

By the test results, a failure envelope may be constructed in the V-H-M space for a particular geometric condition as shown in Fig.15. The envelope defines a region inside which all allowable loading combinations must lie. When the test data with negligible eccentricity are projected onto a M=0 plane, Fig.16 is obtained. As it is difficult to control the vertical loading point to a prescribed position, the eccentricity of the each data point in the figure differs slightly but within the range of $-0.1 < e/B < 0.1$. For the convenience, the data with positive e/B are plotted in the upper half and the data with negative e/B are plotted in the lower half of the figure. Plotted data group on the plane has a shape of cross section of a spindle. The maximum horizontal load can be found at vertical load level of approximately one half of the maximum vertical bearing capacity.

Figure 17 is the failure envelop projected on a V=constant plane. Each test data is shown by a solid circle with numeral which represents the vertical load intensity applied. Projected data group for a similar vertical load intensity level shows a shape of parabola

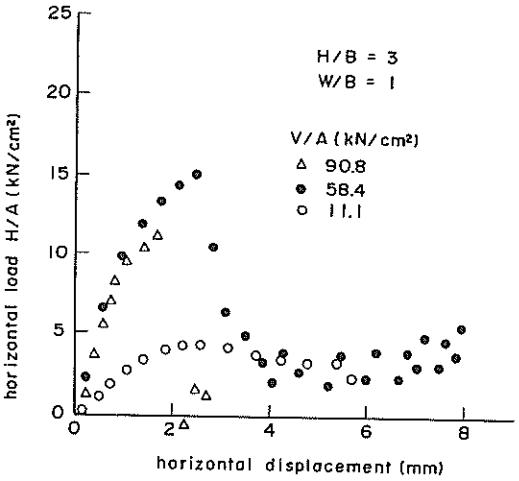

Fig.14 Typical Example of Load - Displacement Relationships

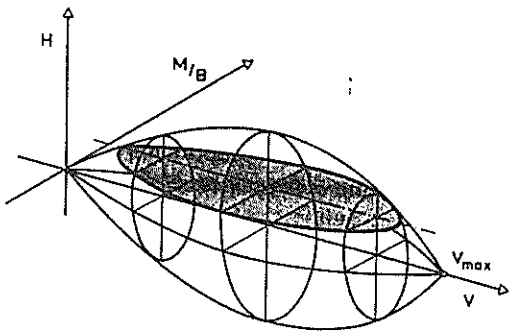

Fig.15 Sketch of Failure Envelope

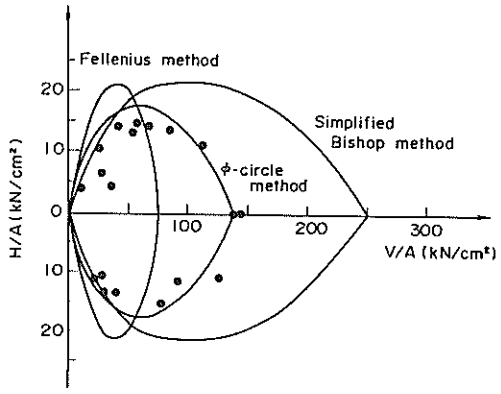

Fig.16 Projected Data on M=0 Plane

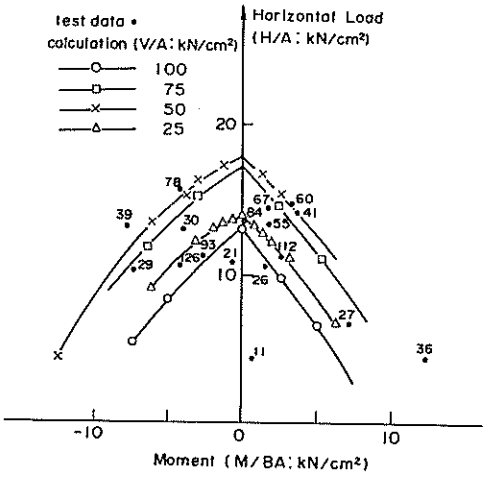

Fig.17 Projected Data on V=constant Plane

convex upward. From this projected image on the V=constant plane and the one in the M =0 plane as already shown in Fig.16, the complete failure envelope for the present test conditions can be constructed in the V-H-M space.

d) comparison with analysis

Three solid curves shown in Fig.16 are the calculated failure envelopes in the V-H plane with M=0 and with internal friction angle ϕ=45 degrees. The calculated failure envelopes by three different slip circle methods are amazingly different in shape. In the present case of the mound with uniform material, the ϕ-circle method with ϕ=45 gives the best fit. As is well known, the Fellenius method gives too small and simplified Bishop

method gives excessive bearing capacity on the V-load axis under vertical loading condition. Whereas the maximum horizontal load component calculated by these methods do not differ too much each other.

The ϕ value is corrected so as to fit the calculated failure loads with test data at the point which represents the maximum vertical bearing capacity. Fitted friction angles are 50 and 41 degrees for the Fellenius method and the simplified Bishop method respectively. Calculated failure envelopes using fitted ϕ values are shown in Fig.18 again together with the test data. Even though the fitted friction angle is used, the Fellenius method is not able to explain the influence of the horizontal load component (load inclination). The simplified Bishop method can be used to estimate the failure envelope if the smaller ϕ value is selected from the triaxial compression tests under varying confining pressure level.

In the actual design practices, most difficult part is the selection of ϕ value. Some trial calculation using the average triaxial ϕ value of 43 degree is suggesting that the ϕ-circle method gives the reasonable but conservative estimation and the simplified Bishop method gives reasonable result as long as the horizontal load is dominant. The test results with analytical investigation were applied for actual constructions of breakwater sitting on huge rubble mound[47),49)].

The results of centrifuge model studies provided fundamental and valuable information

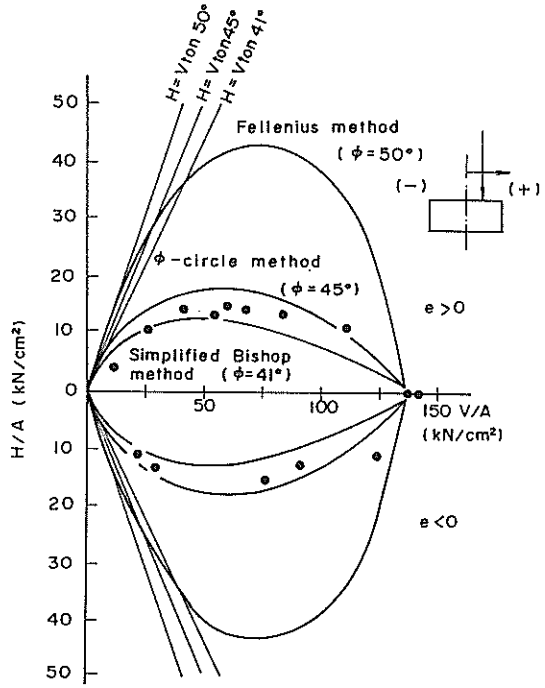

Fig.18 Failure Envelopes obtained by Various Methods

to establish a new design method in which the simplified Bishop method can be used for the unified formula for calculating the bearing capacity of a rubble mound including subsoil under eccentric and inclined loads.

3.2 Bearing Capacity of Clay Ground[53]

Model tests on the bearing capacity of clay ground were conducted from 1985 to 1987. In this test series normally consolidated clay ground of Kaolin clay whose shear strength increases linearly with depth as shown in Fig.19 was manufactured by the continuous long centrifuge operation.

(1) concentric vertical loading test

A series of vertical loading tests was carried out at first changing the footing width to evaluate the vertical bearing capacity of the ground. Figure 20 shows the vertical pressure, V and settlement, δ curves obtained in the tests. It can be seen in all tests that vertical pressure increases with the progress of loading and neither peak pressure nor constant pressure is observed. The bearing capacity is defined as a vertical pressure at bending point of the curve plotted in log - log scale. The vertical bearing capacities of all tests are plotted against the footing width as shown in Fig.21. It is found that the vertical bearing capacity increases with the increase of footing width. The bearing capacities calculated by the Davis and Booker's method[86] are also plotted as a solid curve in the figure. The calculated values are in good coincidence with the experiments. It can be concluded that the Davis and Booker's method reasonably explained the effect both of the footing width and of strength increase with depth on the vertical bearing capacity.

(2) eccentric and inclined loading test

A series of vertical and horizontal loading tests was performed to investigate influence of the load inclination on the bearing capacity. Model ground tested is schematically shown in Fig.22. After the self weight consolidation in high acceleration field of 50 g, the model footing floating above the ground during consolidation was placed on the sand mound by lowering the water depth, and was immediately subjected to horizontal force by means of the electric motor jack.

The loading tests were carried out under various vertical pressures up to the vertical bearing capacity to construct the failure envelope in the vertical and horizontal force space as shown in Fig.23. In the figure, all test data are normalized with respect to $A * C_0$ in which A and C_0 are sectional area of the footing and undrained shear strength at the ground surface respectively. Although number of test results is limited, it can be seen that a failure envelope projected to the V-H plane has a form in parabolic shape. Bearing capacity calculated by means of Vaughans' method[87] and slip circle method are also plotted in the figure. The slip circle method overestimates the bearing capacity and fails to explain the effect of strength increase with depth. The Vaughans' method, on the other hand, reasonably explains the effect of load inclination. The failure envelope of the clay ground is similar to that of sand ground except comparatively high horizontal resistance under small vertical pressure.

This series of test results were employed in the development of a new type breakwater in Kumamoto Port, where relatively light caisson can bear the wave force by the working of the cohesion at the ground surface. This type of breakwater can be applicable to inland sea areas with relatively small wave force, but can reduce construction expense for soil improvement.

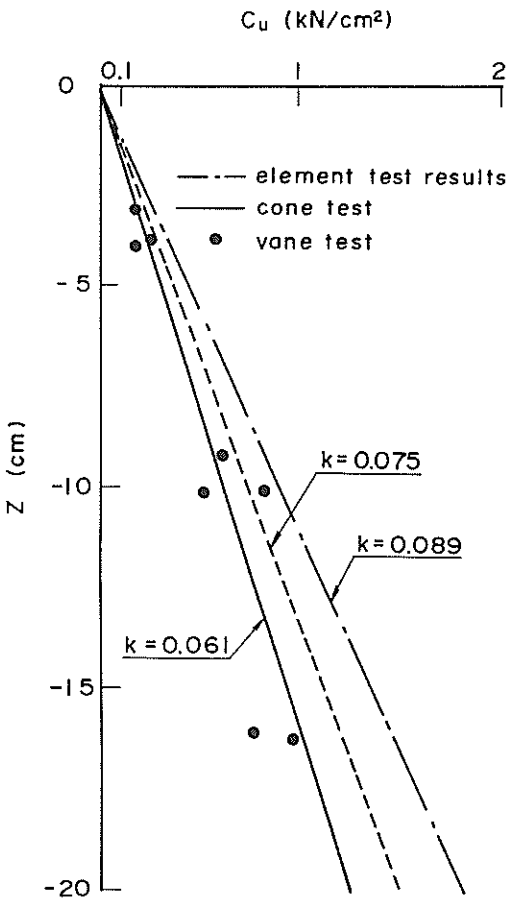

Fig.19 Shear Strength Distribution along Depth

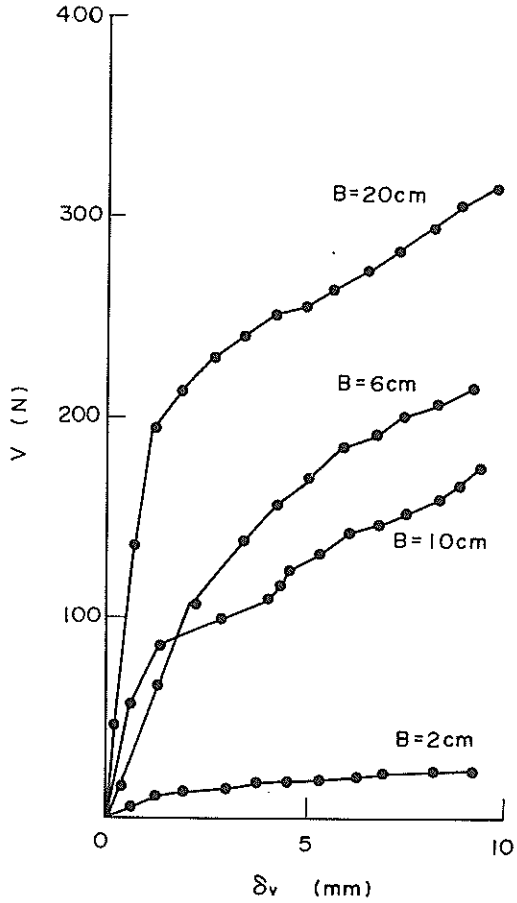

Fig.20 Vertical Pressure and Settlement Curves

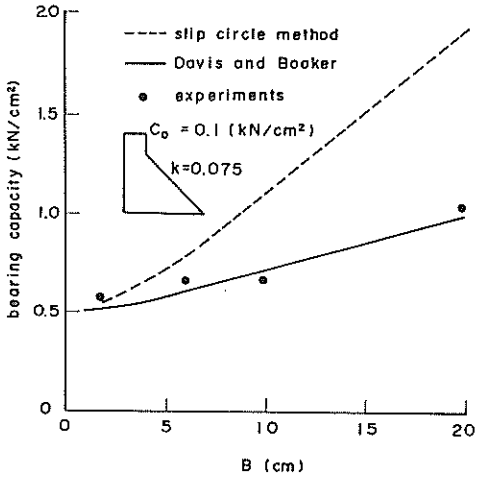

Fig.21 Effect of Footing Width on Bearing Capacity

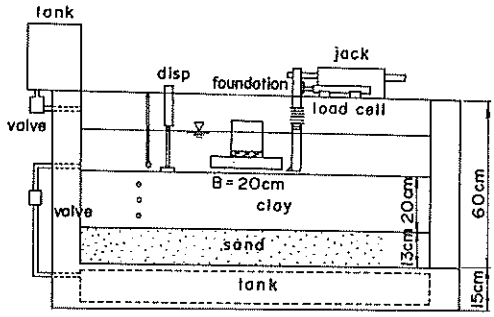

Fig.22 Model Setup

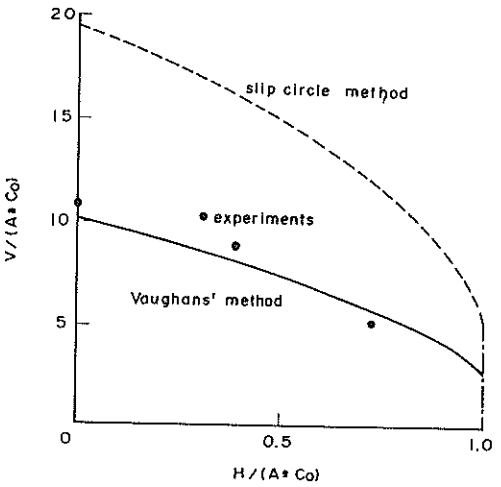

Fig.23 Failure Envelope in V-H Plane

3.3 Behavior of Fabric-Reinforced Clay Ground under Embankment[54),55)]

In Japanese coastal area, difficult problems due to stability or settlement are often encountered in the constructions of temporary roads or containing dikes on the normally consolidated clay ground. To cope with these problems, reinforcement using geotextile is frequently used. To investigate the improvement effect of fabric on normally consolidated clay ground and to clarify the improving mechanism, a series of centrifuge model tests was carried out to simulate and compare the behavior of the reinforced and unreinforced soft clay soil under a variety of embankment configurations. This study was performed to investigate cause of failure of temporary dike during the construction on soft clay ground at a certain port.

(1) General descriptions

A series of model tests was carried out for three different configurations, Type 1 to Type 3 as shown in Fig.24 and Table 3. Type 1 corresponds to an embankment construction on a normally consolidated soft clay where an unwoven fabric is spread in excess of the entire width of the embankment. For the Type 1, comparisons are made between reinforced and unreinforced cases and also for drained and undrained loading conditions. Type 2 corresponds to a wider embankment on a normally consolidated soft soil where a construction of a small containing dike precedes the construction of the main body of the embankment. For this case, an unwoven fabric is placed in excess of the entire width of the containing dike but not under the major body of the embankment.The conditions for Type 1 and 2 are often encountered in practice. In addition to the above mentioned cases, Type 3 is carried out to see the difference in the failure mechanism. This corresponds to a vehicle load or a foundation load acting on the top surface of a reinforced embankment on an over consolidated clay. Since the detail has been described in the original papers[54),55)], only test results of Type 1 is presented here.

(2) test results

A typical model setup for the test series of Type 1 is schematically shown in Fig.25. The clay used in the series of model tests is Kaolin clay and the selected model fabric is an unwoven fabric made of polyester whose major characteristics are listed in Table 4. In

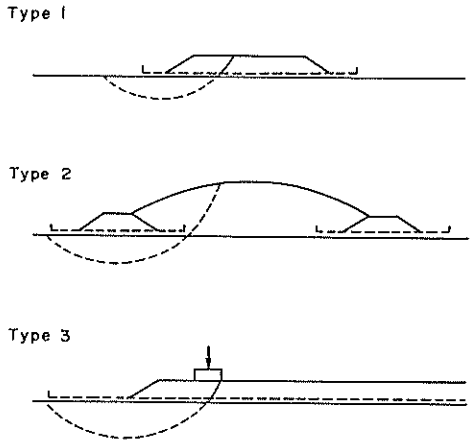

Fig.24 Configurations of Model Tests

Table 3 Test Conditions

	reinforcement	loading
Type 1–U–U	unreinforced	undrained
Type 1–R–U	reinforced	undrained
Type 1–R–DU	reinforced	drained
Type 2–R–U	reinforced	undrained
Type 2–R–DU	reinforced	drained
Type 3–U–U	unreinforced	undrained
Type 3–R–U	reinforced	undrained

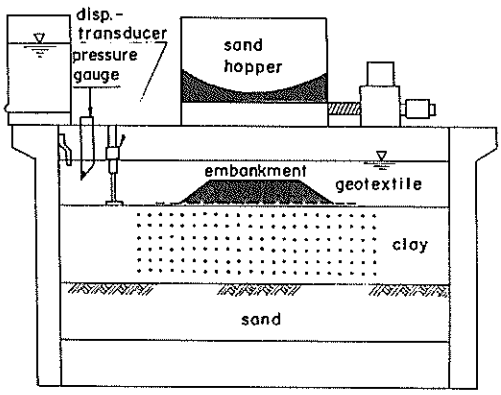

Fig.25 Setup of Model Ground

Table 4 Characteristics of Fabric

thickness (mm)	strength (N/5 cm)	strain at failure (%)
0.038	36	135
elastic limit (N/5 cm)		tensile stiffness (MN/m^2)
12.5		53.1

the test, the thickness of the soft clay is around 20 cm. The undrained shear strength along the depth is determined by means of in-flight vane shear tests and cone penetrometer tests and already shown in Fig.19.

After the self weight consolidation, the embankment construction was simulated during flight by pouring the sand on the ground surface by a special remote controlled sand hopper. The embankment height was increased to the maximum height within 2-3 minutes under a practically undrained condition.

In the unreinforced embankment construction (Type 1-U-U), a failure surface passing through the embankment was clearly found. On the contrary, an embankment (Type 1-R-U) reinforced by the fabric settled uniformly as a whole into the ground with increasing fill height under undrained condition. Therefore it was difficult to determine the point of failure. The critical height of the embankment was determined at a sharp bend in the relationship between the fill pressure and the maximum horizontal displacement along the vertical line at the toe of the embankment. Even after the fill height was increased in ex-

cess of the critical height, there exhibited no sign of fabric or fabric-soil interface failure. This was confirmed later by direct observation of the fabric after removing the embankment. It means that the failures of the embankment with and without reinforcement are caused by the foundation failure.

Critical heights of the unreinforced (Type 1-U-U) and reinforced (Type 1-R-U) embankments are 1.5 cm and 2.5 cm respectively. If the embankment is constructed slowly, the critical height of the embankment can be larger due to strength increase of the clay. In Type 1-R-DU test, the embankment is constructed slowly in steps up to 4.8 cm without any sign of failure. After that, the embankment height is increased rapidly under undrained condition, and the foundation failure is observed at an embankment height of approximately 9.6 cm.

For each test case, the displacement vector loci during undrained loading up to the critical height are shown in Fig.26. Sand is poured continuously even after the foundation failure. Fig.27 shows the displacement loci in the ground after the failure of the foundation soil. In these figures, solid lines represent shear strength profiles of the ground just before the undrained loading and broken lines in Type 1-R-DU represent original strength profiles.

In Type 1-U-U, the maximum horizontal displacement for the critical height appears at the ground surface at the toe of the embankment and the magnitude is approximately 10 mm. The failure zone where large horizontal displacements develop is relatively small: 8 cm wide and 2 cm deep. The failure zone does not expand by the further loading and the central portion of the embankment body shows almost no settlement.

In Type 1-R-U, the magnitude of the maximum horizontal displacement at the toe is also approximately 10 mm but it appears 2-4 cm below the ground surface. Horizontal dis-

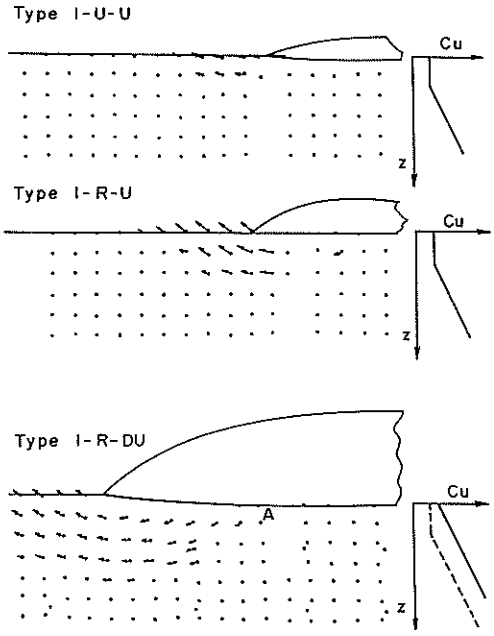

Fig.26 Displacement Vector Loci at Critical Height (Type 1)

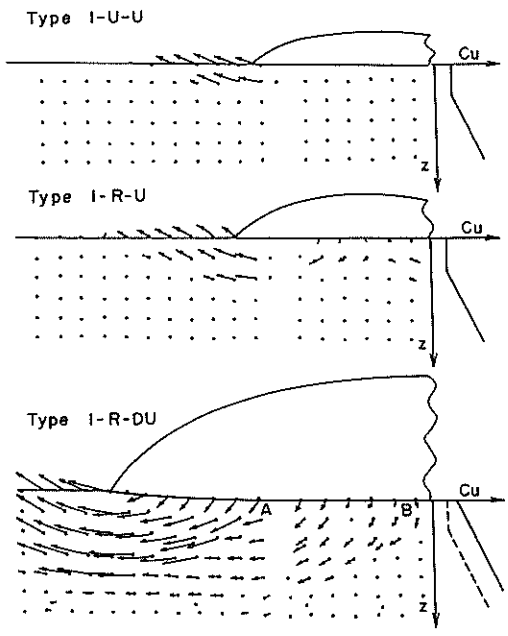

Fig.27 Displacement Vector Loci after Failure (Type 1)

placement at the ground surface is smaller than that. The zone of failure is deeper and wider in comparison with the companion unreinforced case. With continuing sand pouring above the critical height, the central portion of the embankment also starts to settle and finally the entire embankment seems to penetrate into the soft soil.

In the drained loading stages up to 4.8 cm height of Type 1-R-DU, a horizontal displacement of approximately 4 mm develops at the toe of the embankment but at the same time, the embankment settles uniformly about 8 mm due to the consolidation of clay. In the subsequent undrained loading, the magnitude of the horizontal displacement is about 6 mm, and it appears at a depth of around 4 cm. Fig.26 suggests that the failure zone is local around the toe of the embankment and the central portion of the embankment does not settle until the critical height. However, with continuing sand pouring, the entire embankment starts to settle forming a larger zone of failure as shown in Fig.27.

(3) discussion

The critical embankment height for the reinforced case is much higher than that for the unreinforced embankment. The calculations of slip failure are carried out by the Fellenius method of slices to explain this difference. It is suggested by many research workers that the reinforcement effect is to be accounted for in the slip circle analysis by introducing a concentrated force acting at the intersection of slip surface and reinforcement to increase the resistance moment. For this conventional calculation, the concentrated force is assumed to be the sum of fabric-soil interface shear which is smaller than the tensile strength of the fabric in the present model test. The calculated factor of safety is around 1.3 and is too high to explain the critical height of the reinforced embankment. The factor of safety for the foundation failure mode is calculated on a slip circle which approximates the measured slip surface on the conditions of no fabric force and no shear resistance of embankment sand. The calculated factor of safety is around unity and is a much more reasonable value.

The slip surface in the unreinforced case lies in the soft top surface layer, whereas, in the reinforced case, the slip surface travels into the N.C. layer where the shear strength increases with depth. This is the apparent reason for the increased embankment height due to reinforcement. The difference in the position of the slip surface seems to be attributed to two reasons. One reason is that the fabric gives a restraint on the development of horizontal displacements and prevents local failure.It implies that the embankment tends to behave as a unit foundation due to the reinforcement. Another reason is a direct consequence of the first reason. Due to the restraint given by the fabric, the direction of the major principal stress changes at the bottom of the fabric which is in contact with the clay. This is analogous to the change in base roughness of the foundation from smooth (unreinforced) to rough (reinforced). In the present case the tensile stiffness and the flexural rigidity of the fabric are not so large. The reinforced embankment is considered to have behaved as a flexible foundation with a rough base.

In the drained loading, the reinforced embankment gives a large critical height in comparison with undrained loading condition. At the critical height, the potential slip surface passes through point A in the Fig.26. However, with increasing height, the embankment is still stable and at the embankment height of 12 cm, displacement vector loci shown in Fig.27 suggest that the large slip surface passes through point B. After removal of the embankment, there was no sign of elongation of the fabric at point A. It again suggests that the fabric functions to give a confinement on the behavior of the embankment and reinforced embankments tend to behave as a unit.

3.4 Bearing Capacity of Improved Ground by Sand Compaction Piles[57)-60)]

Sand compaction pile method (SCP) has been applied to improve the soft ground often found in the Japanese coastal area. When the method is applied to improve clay deposits, the improved ground is often called a composite ground. The authors investigated the bearing capacity of the submarine composite ground with low a_s (a_s : the replacement area ratio) improvement under a combination of vertical and horizontal loads.

(1) test procedure

The setup of model ground is shown in Fig.28. A thick normally consolidated clay layer of Kaolin is reduced in scale and prepared in a strong specimen box which has the following inside dimensions: 30 cm deep, 10 cm wide and 50 cm long. All the model tests were carried out in the 50 *g* field. In order to reflect the prototype loading condition of the breakwater or revetments to the model test, it is most appropriate to apply the vertical load component in advance to applying the horizontal load component. The vertical load component was applied by quick lowering of the water level. The horizontal component was applied immediately after that by means of the horizontal loading jack.

Test conditions and results of a series of tests are summarized in Table 5. The vertical load component, V and horizontal load component, H are the loads where the improved ground comes to yield. Load inclination is the inclination of the resultant load at yield which is measured from vertical. Therefore test No. 1 is the vertical bearing capacity test with zero inclination and No. 3 to No. 5 are the tests for the inclined loading.

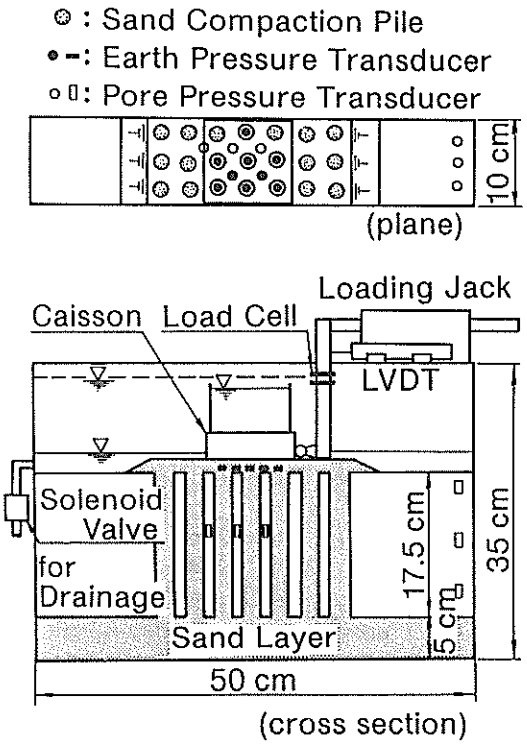

Fig.28 Setup of Model Ground

Table 5 Test Conditions

Test No.	1st Load (kN)	Total Load at Yield		Load Inclination (deg)
		V. Load (kN)	H. Load (kN)	
1	0.10	0.60	0	0
3	0.10	0.10	0.057	29.7
4	0.10	0.29	0.088	16.5
5	0.10	0.45	0.070	8.8

(2) test results

In test No.1, vertical loading test, the load increases with increasing settlement and neither peak nor the final constant load is observed as shown in Fig.29. The bearing capacity of the improved ground is determined as a yield of the ground. The yield load of the ground is defined by the intersection of the initial tangent line of the curve and the tangent line at the straight portion of the curve at the larger settlement. The arrow in the figure shows the position of the bearing capacity thus determined.

For the inclined load tests, horizontal load H - horizontal displacement δ_h curves are obtained and shown in Fig.29. In test No. 3 for the largest load inclination, H increases with increasing δ_h but the load becomes constant after δ_h reaches a certain value. The bearing capacity for this particular case is therefore determined as this final constant value. Whereas the H - δ_h curves for the smaller load inclination do not show either peak or the final constant value. The bearing capacities for these cases are determined by the intersection of two tangent lines. As shown in the figure, it is known that the horizontal component of the bearing capacity is highly dependent upon the load inclination.

Figure 30 is the photograph taken after the load test (Test No. 1) to observe the deformation of sand piles directly. Shear planes and the sliding wedge are clearly observed in the central three rows of sand piles. The piles outside the wedge are deformed at their tops by the penetration of wedge but the overall improved ground does not reach the general shear failure.

The vertical load component, V and the horizontal load component, H at yield or failure of the improved ground for all the tests are plotted in Fig.31 to obtain the bearing capacity envelope on the V - H plane. The failure envelope similar to this has been also found previously for the bearing capacity of sand under the inclined load (Fig.16). The horizontal load which can be supported by the improved ground increases with the increasing vertical load. However, when V reaches around a half of the vertical bearing capacity, H becomes maximum and decreases with further increase of V level.

(3) Comparison with Practical Design Technique

Several failure criteria for the composite ground have been proposed and employed in the routine design for many years in Japan. The bearing capacity is calculated by the Fellenius method of slip circle analysis combined by a shear strength expression and shown by a solid curve in Fig.31. The curve gives the cigar shaped bearing capacity envelope in the V-H plane and is acceptable both qualitatively and quantitatively.

Also calculated and shown by a solid straight line in Fig.31 is the simple sliding failure of the foundation on the surface of sand mound. For this failure mode, the maximum horizontal load is calculated as a product of the effective weight of the foundation and the factor of friction of the sand mound, $\tan \phi'$. As is observed in the figure, the results obtained both by calculation and experiment are in perfect accordance for the sliding failure.

Full scale loading test was also performed in 1986 to 1988 in which SCP improved ground was subjected to vertical load to failure, and it was found failure load was well coincidence with the calculation[60),88)]. From the model and field test results, the validity

and practical use of the current design procedure is confirmed as long as it is used with the adequate design constants.

This series of test results was employed in the development of design formula of improved ground by sand compaction pile method with low replacement area ratio.

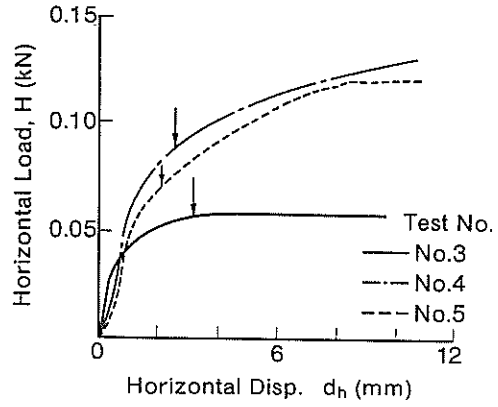

Fig.29 Horizontal Load - Displacement Curve

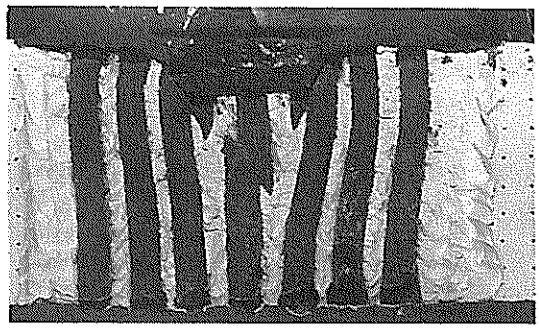

Fig.30 Failure Mode of Compacted Sand Piles (No.1)

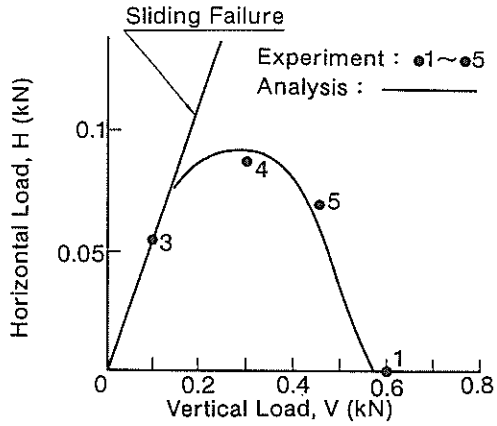

Fig.31 Bearing Capacity Envelope in V-H Plane

3.5 Horizontal Resistance of a Pile in Sand[62)-64)]

The centrifuge modeling of the behavior of a long pile and pile groups in a slope or in a layered soil system was investigated which are often encountered in the port structures in Japan. In this article only lateral load tests of a sufficiently long pile embedded in a horizontal layer of uniform dense sand was described.

(1) model ground

The model setup is schematically shown in Fig.32. All the model tests were carried out in a strong specimen box which has inside dimensions 46 cm deep, 20 cm wide and 50 cm long.

Plate piles are used for the model tests. Three materials of different elastic moduli, E are used to adjust the flexural rigidity, EI of piles, i.e. mild steel, aluminum and acrylic resin. Strain gages are installed at both faces of the plate piles at 12 levels in average to determine the bending moment distribution along the pile length. A free-headed model pile is fixed at the bottom end by a clamp to stand by itself except for preliminary test series (series I in Table 6).

The sand used is fine grained uniform Toyoura sand having uniformity coefficient, U_c of 1.38 and the effective grain size, D_{10} of 0.13 mm. The model ground of air dried Toyoura sand is prepared in the strong box on a laboratory floor by means of the multiple sieve method of sand raining. The average relative density of the sand is 87 %. The top surface of the ground is carefully leveled by sucking sand particles by a vacuum cleaner. After the sand ground is prepared, the pile is loaded laterally at the top by the motor jack with a constant displacement rate of 0.6 mm/min at a high acceleration field. The lateral load is measured by a cantilever-type load cell during the test. Also measured are the displacement of the pile top and moment along the pile.

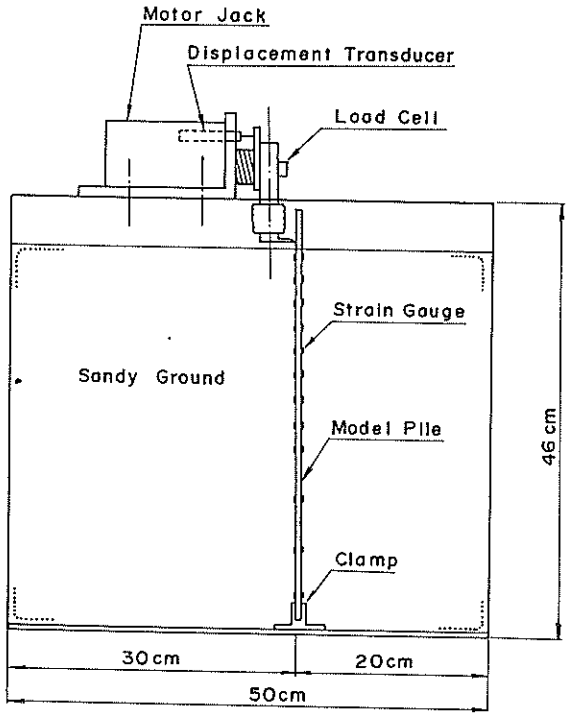

Fig.32 Setup of Model Ground

Table 6 Test Conditions for Model and Prototype

Test Series	MODEL TEST CONDITIONS						PROTOTYPE CONDITIONS		
	Embedment L_m (cm)	Pile width B_m (cm)	Pile thickness t (cm)	Pile Rigidity EI_m (N·m²)	Loading Height h_m (cm)	Acceleration n (g)	Embedment L_p (cm)	Pile Width B_p (cm)	Pile Rigidity EI_p (MN·m²)
I	40.0	2.0	0.5	15.2	0.4	40	1600	80.0	38.8
	20.0	2.0	0.5	15.2	0.5	39.9	798	80.0	38.6
	10.0	2.0	0.5	15.2	0.4	40.1	401	80.1	39.1
II	40.3	3.2	0.8	88.2	0.6	25.7	1036	82.2	38.5
	39.5	2.8	0.7	51.5	0.65	28.6	1129	80.1	34.5
	40.7	2.0	0.5	15.2	0.4	40.2	1636	80.4	39.7
	36.0	1.6	0.4	6.0	0.3	49.2	1771	78.7	35.1
	31.8	1.2	0.3	2.0	0.35	66.4	2112	79.7	38.9
	30.1	1.0	0.25	1.03	0.15	77.2	2323	77.2	36.7
III	25.7	2.0	0.2	1.03	0.4	39.9	1025	79.8	2.61
	40.2	2.0	0.23	5.83	0.5	39.8	1600	79.6	14.6
	40.7	2.0	0.5	15.2	0.4	40.2	1636	80.4	39.7
	40.7	2.0	0.8	59.0	0.45	40.9	1665	81.8	165.0
	40.7	2.0	0.8	202.0	0.35	39.9	1624	79.8	511.0
IV	40.5	0.52	0.5	3.9	0.3	40.9	1656	21.3	10.9
	40.8	1.11	0.8	33.9	0.4	41.0	1673	45.5	95.7
	40.7	2.0	0.5	15.2	0.4	40.2	1636	80.4	39.7
	40.1	2.8	0.7	51.5	0.25	40.1	1608	112.3	133.0

(2) test results

A prototype pile conditions selected as a standard for the model tests are 80 cm wide and sufficiently long plate pile with flexural rigidity, *EI* of 39 MN·m². All the test conditions are listed in Table 6. The dimensions and flexural rigidity of a pile with suffix m denote the actual model conditions and those with suffix p denote those for prototype. Although four series of model tests were performed, only the test series of modeling of models is reviewed here.

Modeling of models is a common practice to investigate the scaling relations by testing structures of different scale ($1/n_i$) in different acceleration ($n_i\ g$) such that the product of size and acceleration becomes constant. In the series on modeling of models, a standard prototype pile is scaled down to 6 different sizes and tested in 6 different accelerations. Relationships between the lateral load and the pile top displacement of all the tests are compared in Fig. 33. The magnitude of load and displacement in this figure is those of model scale, H_m and $y_{top,m}$. The curve of each test shows nonlinear relationship and naturally differs each other. Measured values are converted into those at assumed prototype scale, H_p and $y_{top,p}$ and replotted in Fig.34. The six curves coincide perfectly.

The plots of moment distributions, M_p along the depth x_p measured from the ground surface in prototype scale also show perfect coincidence as shown in Fig.35. Modeling of models revealed a perfect coincidence of the pile behavior regardless of the actual model scale. The validity and capability of the centrifuge modeling is demonstrated.

Measured M_p-x_p curve is fitted by polynomial function and differentiated twice to obtain the soil resistance, p and integrated twice to obtain the deflection of pile, y at an arbitrary load level. The p-y relations in logarithmic scale as shown in Fig.36 are thus obtained at $x_p = 2$ m. The test data suggest that the soil resistance, p is proportional to square root of the deflection. The p-x_p relations obtained in the later test series are plotted in Fig.37. Soil resistance increases with depth irrespective of the difference in the rigidity of the piles. This relation, $p = k_s \times y^{0.5}$ is exactly the relation found in the early 1960's by the large scale model tests for sandy ground[89]. Later, this expression is found

also applicable to the clay ground where shear strength increase with depth. Coefficient k_s of soil resistance is constant for a certain combination of pile and soils condition The method of calculating load and deflection of laterally loaded pile based on this relationship (PHRI method) has been adopted for long by the Japanese Technical Standards for Port and Harbour facilities[90] and the validity of the method has been confirmed at a number of practices.

3.6 Consolidation Behavior of Soft Clay with Fabri-packed Sand Drain[60)-70)]

Vertical drains have been widely used for soft clay grounds to accelerate consolidation

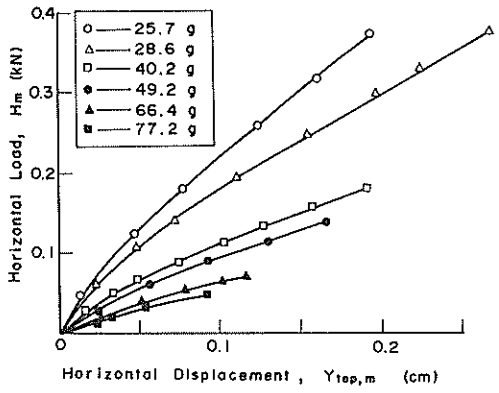

Fig.33 Lateral Load - Pile Top Displacement (model scale)

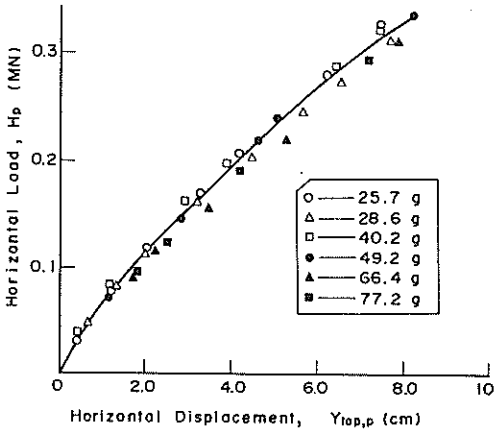

Fig.34 Lateral Load - Pile Top Displacement (prototype scale)

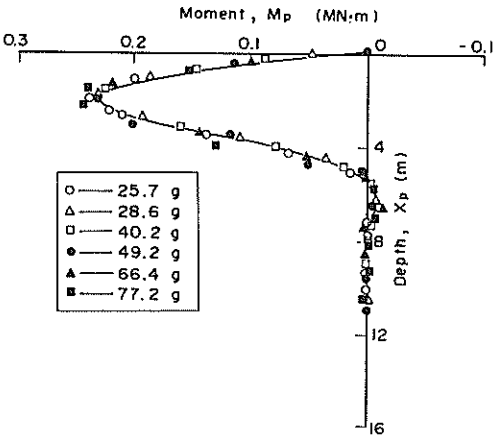

Fig.35 Moment Distributions (prototype scale)

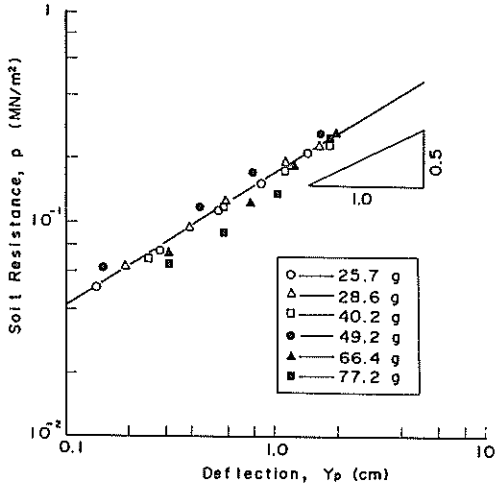

Fig.36 p-y Relation

and to minimize residual and differential settlements. In the case in which a construction site has an extremely high water content, sand piles for the ordinary vertical drain method can not stand by themselves and may fail to function as a drainage path. To cope with the problem, fabri-packed sand drain, which is sand drain wrapped by an envelope made of geotextile, is proposed as one of alternatives. The geotextile is expected to stabilize the sand pile but might cause a concentration of the fill pressure to the sand pile if it has an excessively high tensile rigidity.

A series of centrifuge model tests was performed to investigate the effect of the geotextile on the stability of the sand pile and on the consolidation behavior of the improved ground.

(1) test procedure

This model test was performed for the Tokyo International Airport (Haneda) Offshore Expansion Project[91] and model ground was simulated for the prototype ground condition as much as possible. Many fabri-packed sand drains are constructed at a regular interval in the prototype. In the model test only one drain surrounded by a soft clay deposit was simulated for ease of model preparation. The model ground was prepared in a perspex cylinder at a scale ratio of 1/25. The setup of the model ground is schematically shown in Fig.38.

The model ground was brought to an acceleration field of 25 g and allowed to consolidate by its enhanced self-weight. During the consolidation, the settlements at the fill surface and pore water pressures within the model ground were monitored. After reaching 90% consolidation, the centrifuge was stopped to end the test. After the model ground was pushed out from the cylinder, the deformation of the sand pile was observed. Water contents were also measured at several points to obtain the distribution within the ground.

Seven model tests, including a case without a fabric reinforcement, were carried out changing the tensile rigidity of the geotextiles as shown in Table 7.

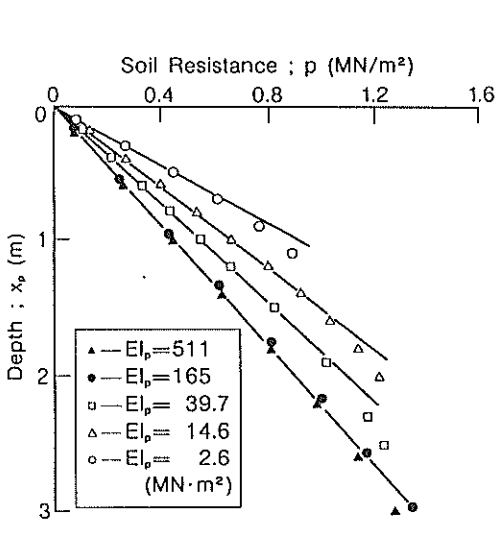

Fig.37 Change of Soil Resistance with Depth

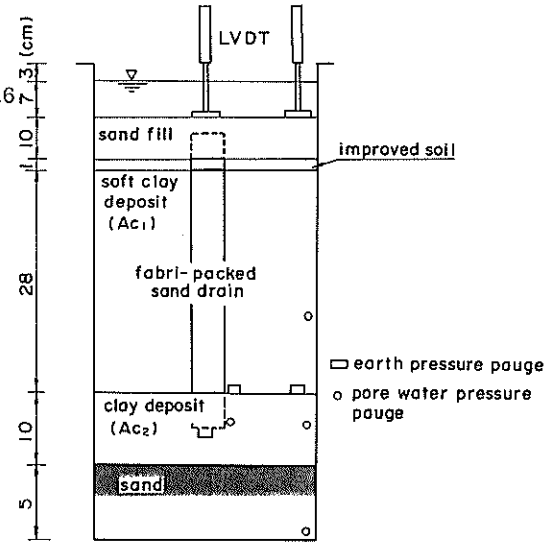

Fig.38 Modeling of Prototype in Centrifuge

Table 7 Test Case

	prototype	1	1'	2	3	4	5	6
material	Polyethylene	non-woven cloth						
tensile rigidity (N/5 cm/%)								
horizontal	18	15	15	88	140	140	160	——
vertical	46	160	160	175	50	50	15	——
strength (N/5 cm/%)								
horizontal	516	443	443	403	2930	2930	2170	——
vertical	1020	2170	2170	270	1390	1390	443	——
average vertical strain at max. earth pressure (%)		36.1	36.1	33.9	29.2	32.5	31.1	29.3

(2) test results

Figure 39 shows time settlement curves during the consolidation in case 1. The two curves obtained at the top of the sand pile and at the clay surface completely coincide during the consolidation, which shows no differential settlement took place even in the composite ground consisted of the soft clay and the relatively stiff sand pile reinforced by the fabric envelope.

Figure 40 shows the development of the sand pile deformation. The sand pile started to expand in diameter to follow the vertical consolidation settlement as long as the settlement remains relatively small. But when a large settlement takes place, the pile has a tendency to deform like a snake to absorb the large vertical compression. Measured elapsed times for completion of the consolidation for all case are compared with that calculated by Barron's equation. The measured values are in good agreement with the calculated values[92]. This ensures that such a heavily deformed sand pile can still function as a drainage path, even in a non-packed case.

Figure 41 shows the stress concentration ratio against the tensile rigidity of the geotextile in the tangential direction. In the figure, the stress concentration ratio, n is defined as a ratio of the average effective vertical stress on the sand against that on the clay. The ratio, n for the non-packed case is also estimated and plotted by a cross on the vertical axis. It should be noted that the stress concentration of about 1.5 takes place even in the non-packed case. Although these values scatter, the ratio increases almost linearly with the tensile rigidity of the geotextiles.

The influence of the stress concentration on the consolidation settlement can be evaluated by the equation, whose validity has been confirmed for the improved ground by sand compaction piles[93]. The influence can be estimated 2 % by substituting the stress concentration ratio of 1.6 and replacement area ratio of 0.03. Therefore it can be concluded that the settlement decreases at the Haneda site due to the stress concentration could remain within 5% as long as the tensile rigidity dose not exceed about 200 N/5 cm/%.

The study reveals that the geotextile functions well to stabilize the sand pile in the extremely soft clay ground. The stress concentrations resulting from the tensile rigidity of the geotextiles evaluated are smaller than anticipated and may not cause undesirable settlement.

As the applicability of the fabri-packed sand drain is confirmed by the centrifuge model study, the method is employed in the Haneda Project. The effectiveness of this method, as well as the stability performance, have been confirmed at site. The consolidation behavior will be evaluated soon by the field measurements and will be published elsewhere.

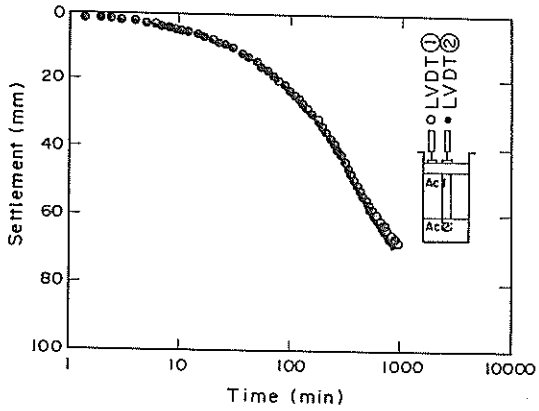

Fig. 39 Time Settlement Curves

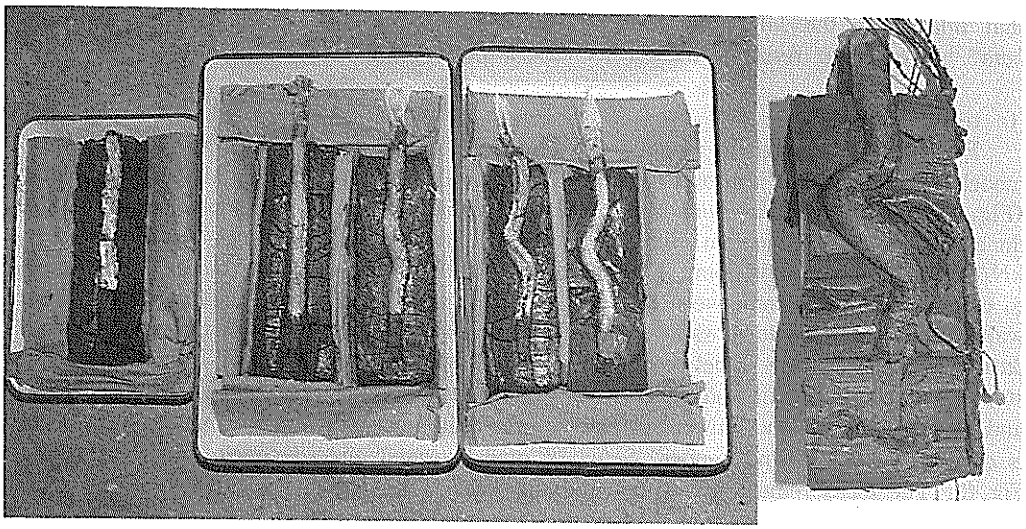

Fig.40 Progress of the Sand Pile Deformation

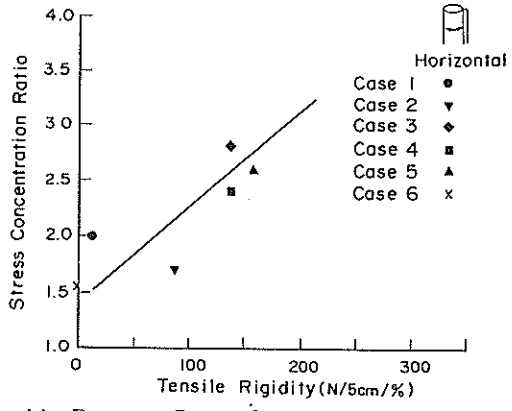

Fig.41 Relationship Between Stress Concentration Ratio and Tensile Rigidity

3.7 External Stability of Improved Ground by Deep Mixing Method[72,73),77)]

Deep Mixing Method (DMM) is a kind of in-situ admixture stabilization technique using such stabilizing agent as quick lime, slaked lime, cement, or a combination of lime, cement, slag, or gypsum. The method was invented and developed by the Port and Harbour Research Institute to improve soft marine deposits. Due to the quick strength increase and extraordinary high shear strength of the improved soil, DMM has become one of the most effective soil improvement techniques for near-shore and off-shore constructions.

The in-situ treated Japanese marine clays by DMM are characterized by a high unconfined compressive strength of the order of 1 MN/m^2, small strain at failure in the order of 0.1 %, relatively low tensile strength and low permeability. Therefore the treated soil is considered not to be a part of the ground but to be a rigid structural member buried in the ground in order to deliver the external loads to a reliable stratum.

In the calculation of the stability of the improved ground, rigorous determination of the stresses acting on the boundary of the buried structure is important. A series of model tests has been carried out for the buried structure resting on the reliable sandy layer and that floating in the soft clay. Since the details have been described in the original papers[72,73)], only test result of the former case is presented here.

(1) test procedure

Bakelite stiff enough to model treated soil whose unit weight is 1.39 g/cm^3 is used to model a rigid buried improved ground. Long walls of a model rigid buried structure (Fig.42) is placed on the sand layer in the prescribed position in the specimen box. Kaolin clay remolded by vacuum mixer is poured on the sand layer and pre-consolidated at 10 kN/cm^2 in a laboratory floor. Following pre-consolidation, specimen box is disassembled to embed short walls in-between long walls. In the self weight consolidation at 50 g, short walls are set between long walls independently from long walls so as to allow free consolidation of the soft clay in-between long walls. After the consolidation, centrifuge is once stopped to connect long and short walls tightly as it is the case of actual improvement and to place mound and caisson in place. Acceleration is increased again and back filling is carried out using sand hopper. Setup of model ground and specimen box are shown in Fig.43. The measurement of the boundary stresses is carried out by earth pressure transducers and pore water pressure transducers embedded in the structure.

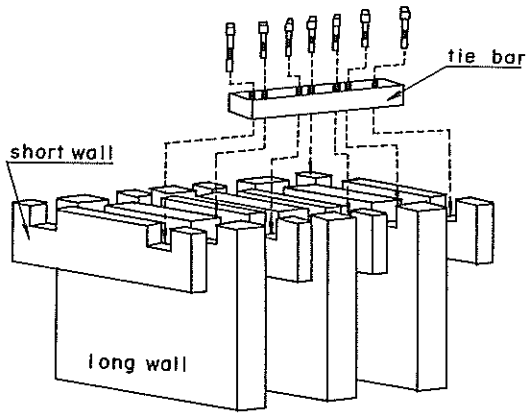

Fig.42 Model of Treated Soil Walls

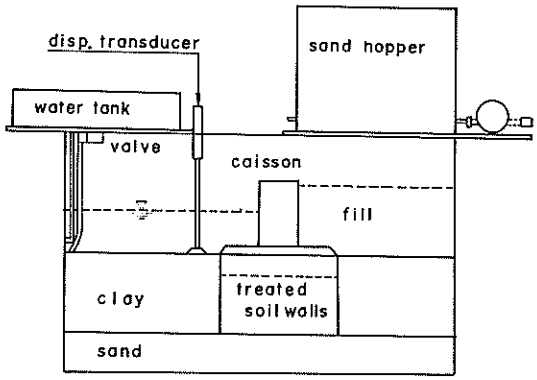

Fig.43 Setup of Model Ground

(2) test results

In the centrifuge tests, the depth of clay is 10 cm, the long walls reach the underlying sand layer, the height of short wall is 3cm, the thickness of long wall is 2 cm and that of short wall is 1cm. Difference is in the width of long wall; the width of long wall is 10 cm for case A and 15cm for case B. It means the factor of safety against external stability is higher in case B. Factor of safety for sliding is 1.0 for case A and 1.4 for case B.

Measured total earth pressure (TEP) and pore water pressure (PWP) are shown in Fig.44. TEP and PWP underneath the fill respond quickly to filling and whose magnitude is quite reasonable in case B (Fig.44b)). However, in case A, TEP and PWP underneath the fill respond only to first filling (Fig.44a)). As is already explained, factor of safety for sliding in case A is around unity. Disagreement between applied vertical stress and measured pressure increment in the case A seems to be due to the horizontal displacement of the buried structure. TEP and PWP on the front of the improved ground shows negligibly small increase with filling in both cases. The pressure increases with filling and decreases with the consolidation of the clay is shown in Fig.44c).

Change of horizontal pressures with time and change of contact pressure distributions at the bottom of long wall are clearly shown in Fig.45. Contact pressures at the bottom of long walls are calculated by assuming that the buried structure is rigid and it seats on the elastic springs. The calculated contact pressure distribution based on the horizontal component of earth pressure (solid line in Fig.45 for U=100 %) is steeper than measured one. This is because no account was taken for the vertical component of earth pressure from the fill, shear stress induced in the clay layer on the surface of a improved ground to restrain the rotational movement at the instance of loading, and the negative skin friction in the long run. Contact pressure distribution taking account of vertical component of earth pressure of the fill material and the negative skin friction acting on the treated soil walls is shown by dotted line in Fig.45 also for U=100 %.

From the study, it is know that the design load condition is sensitive to relative movement of a treated ground to surrounding soft soils.

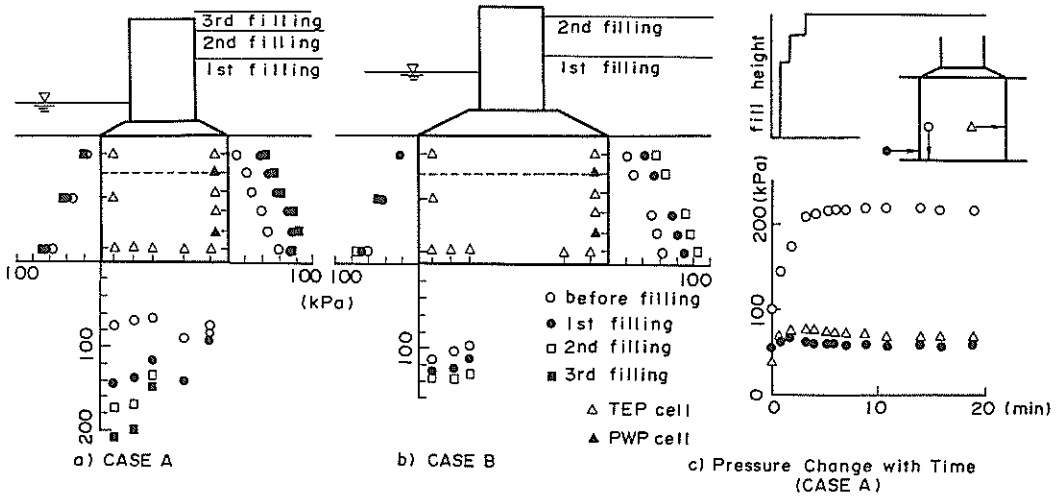

Fig.44 Measured Pressure in the Filling Stage

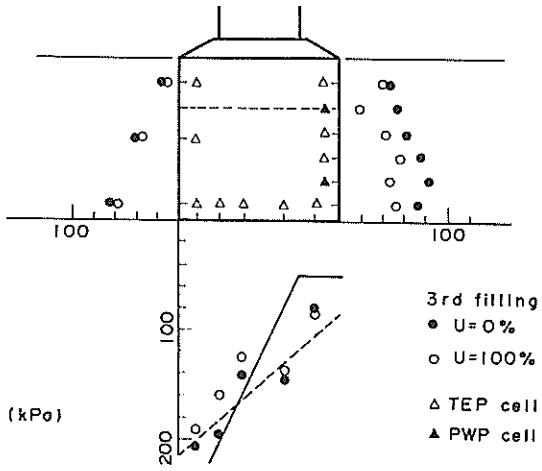

Fig.45 Pressure Re-distribution due to Consolidation

4. Concluding Remarks

Over 14 years the centrifuge at PHRI has been used continuously to investigate a wide range of geotechnical problems. And to date, most part of the researches are on the model formed of remolded soil, but our achievements with remolded soil are important to investigate failure processes, soil-structure interaction, behavior of complex soil systems and so on.

PHRI belongs to the Ministry of Transport which is responsible for the design and construction of port and airport facilities. Great demands exist to simulate not only ideal prototype-scale structures but also the site specific prototypes. The challenging but fairly difficult field of centrifuge application will be one of the major subjects of the PHRI Mark II centrifuge in near future.

Reference

1) SCHOFIELD, A.N.: Cambridge geotechnical centrifuge operations, *Geotechnique* 30, No.3, 1980, pp.227-268.

2) TREASHI, M.: Development of PHRI geotechnical centrifuge and its application, *Report of the Port and Harbour Research Institute*, Vol.24, No.3, 1985, pp.73-122.

3) TERASHI, M.: Application of PHRI geotechnical centrifuge, *Proc. of International Symposium on Geotechnical Centrifuge Model Testing*, 1984, pp.164-171.

4) RANDOLPH, M.F., JEWELL, R.J., STONE, K.J.L. and BROWN, T.A.: Establishing a New Centrifuge Facility, *CENTRIFUGE 91*, 1991,

5) LIU, L.-D. and TANG, J.-H.: A Huge Centrifuge for Geotechnical Studies, *CENTRIFUGE 88*, 1988, pp.33-36.

6) ZHANG, L. and HU, T.: Centrifugal Modeling of the Pubugou High-rise Rockfill Dam, *CENTRIFUGE 91*, 1991, pp.45-50.

7) LIU, L. and GAO, Y.: Experimental Study on Consolidation of Soft Soils under Negative Pressure with Centrifugal Models, *CENTRIFUGE 88*, 1988, pp.181-184.

8) JIA, P.-Z., WANG, W.-H. and RU, L.-A.: The Survey of Conceptual Design for a 450 g-t Geotechnical Centrifuge, *CENTRIFUGE 88*, 1988, pp.17-22.

9) ZHU, W. and LIU, S.: NHRI Geotechnical Centrifuge Operation, *CENTRIFUGE 88*, 1988, pp.49-54.

10) WANG, X.: Studies on the Design of a Large Scale Centrifuge for Geotechnical and Structural Testing, *CENTRIFUGE 88*, 1988,

11) OVESEN, N.K.: Centrifuge Tests of Embankments Reinforced with Geotextiles on Soft Clay, *Proc. of International Symposium on Geotechnical Centrifuge Model Testing*, 1984, pp.14-21.

12) GARNIER, J. and COTTINEAU, L.M.: The LCPC Centrifuge : Means of Model Preparation and Instrumentation (Summary), *CENTRIFUGE 88*, 1988, pp.91-92.

13) SCHOFIELD, A.N. and TAYLOR, R.N.: Development of Standard Geotechnical Centrifuge Operations, *CENTRIFUGE 88*, 1988, pp.29-32.

14) FRYDMAN, S. and BEASLEY, D.H.: Centrifugal Modelling of Riverbank Failure, *Proc. ASCE*, Vol.102, No. GT5, 1976, pp.395-409.

15) DICKIN, E.A.: Stress-displacement of Buried Plates and Pipes, *CENTRIFUGE 88*, 1988, pp.205-214.

16) LEUNG, C.F. and DICKIN, E.A.: Scale Error of Conventional Model Tests, *Proc. of International Symposium on Geotechnical Centrifuge Model Testing*, 1984, pp.133-138.

17) JESSBERGER, H.L. and GUTTLER, U.: Bochum Geotechnical Centrifuge, *CENTRIFUGE 88*, 1988, pp.37-44.

18) SCHURMANN, A. and JESSBERGER, H.L.: Earth Pressure Distribution on Sheet Walls, *CENTRIFUGE 94*, 1994, pp.95-100.

19) Research Activities Faculty of Civil Engineering Period 1988-1989, *Delft University of Technology*, pp.123.

20) LESHCHINSKY, D., FRYDMAN, S. and BAKER, R.: Study of Beam-soil Interaction using Finite Element and Centrifugal Models, *Canadian Geotechnical Journal*, Vol.19, 1982, pp.345-359.

21) BALDI, G., MAGGIONI, W. and BELLONI, G.: The ISMES Geotechnical Centrifuge, *CENTRIFUGE 88*, 1988, pp.45-48.

22) MAENO,Y. and UCHIDA, K.: *Proc. of Coastal Engineering, JSCE*, Vol.37, 1990, pp.754-758 (in Japanese).

23) TANIGUCHI, E., KOGA, Y., MORIMOTO, I. and YASUDA, S.: Centrifugal Model Tests on Reinforced Embankment by Non-woven Fabric, *CENTRIFUGE 88*, 1988, pp.253-258.

24) HONDA, M., TEI, K., SUZUKI, R. and OOKUBO, N.: Effects of Boundary Condition at Container Walls and Pitching Motion in Dynamic Centrifuge Test, *Kajima Technical Institute Annual Report*, Vol.41, 1993, pp.193-198 (in Japanese).

25) MIKASA, M., TAKADA, N., IKEDA, M. and TAKEUCHI, I.: Centrifuge Model Test of Dynamic Consolidation, *CENTRIFUGE 88*, 1988, pp.185-192.

26) MIKASA, M.: Two Decades of Centrifugal Testing in Osaka City University, *Proc. of International Symposium on Geotechnical Centrifuge Model Testing*, 1984, pp.43-49.

27) NAGURA, K., TANAKA, M., KAWASAKI, S. and HIGUCHI, Y.: *Taisei Technical Research Report*, Vol.25, 1994, pp.141-148 (in Japanese).

28) FUJII, N., KUSAKABE, O., KETO, H. and MAEDA, Y.: Bearing Capacity of a Footing with an Uneven Base on Slope : Direct Comparison of Prototype and Centrifuge Model Behavior, *CENTRIFUGE 88*, 1988, pp.301-306.

29) KIMURA, T., NAKASE, A., KUSAKABE, O., SAITOH, K. and OHTA, A.: Geotechnical Centrifuge Model Tests at the Tokyo Institute of Technology, *Technical Report* No.30, *Department of Civil Engineering, Tokyo Institute of Technology*, 1982, pp.7-33.

30) MIYAKE, M., AKAMOTO, H. and ABOSHI, H.: Filling and Quiescent Consolidation including Sedimentation of Dredged Marine Clays, *CENTRIFUGE 88*, 1988, pp.163-170.

31) TOYOZAWA, Y. and HORII, N.: Centrifuge Modeling of Excavations, *Proc. of the 25th Japan National Conference on Soil Mechanics and Foundation Engineering*, *JSSMFE*, 1990, pp. 1505-1506 (in Japanese).

32) MALUSHITSKY, Yu.N.: The Centrifugal Model Testing of Waste-heap Embankments, *Cambridge University Press*, 1981, pp.4-7.

33) SCHOFIELD, A.N.: General Principles of Centrifuge Model Testing and a Review of Some Testing Facilities, *Offshore Soil Mechamics*, 1976, pp.327-339.

34) LEE, F.H., TAN, T.S., LEUNG, C.F., YONG, K.Y., KARUNARATNE, G.P. and LEE, S.L.: Development of Geotechnical Centrifuge Facility at the National University of Singapore, *CENTRIFUGE 91*, 1991, pp.11-17.

35) CHENEY, J.A. and FRAGASZY, R.J.: The Centrifuge as a Research Tool, *Geotechnical Testing Journal*, Vol.7, No.4, 1984, pp.182-187.

36) CLOUGH, H.F., WURST, P.L. and VINSON, T.S.: Determination of Ice Forces with Centrifuge Models, *Geotechnical Testing Journal*, Vol.9, No.2, 1986, pp.49-60.

37) ELGAMAL, A.W., DOBRY, R., LAAK, P.V. and FONT, J.N.: Design, Construction and Operation of 100 g-ton Centrifuge at RPI, *CENTRIFUGE 91*, 1991, pp.27-34.

38) VUCETIC, M., TUFENKJIAN, M.R. and DOROUDIAN, M.: Dynamic Centrifuge Testing of Soil-Nailed Excavations, *Geotechnical Testing Journal*, Vol.16, No.2, 1993, pp.172-187.

39) FRAGASZY, R.J. and TAYLOR, T.: Centrifuge Modeling for Projectile Penetration Studies, *Geotechnical Testing Journal*, Vol.12, No.4, 1989, pp.281-287.

40) THOMPSON, P.Y. and KIM, Y.S.: The Development of a Geotechnical Centrifuge Facility at Tyndall Air Force Base, *CENTRIFUGE 88*, 1988, pp.67-72.

41) CHENEY, J.A. and KUTTER, B.L.: Update on the US National Geotechnical Centrifuge, *CENTRIFUGE 88*, 1988, pp.61-66.

42) KUTTER, B.L., LI, X.S., SLUIS, W. and CHENEY, J.A.: Performance and Insrumentation of the Large Centrifuge at Davis, *CENTRIFUGE 91*, 1991, pp.19-26.

43) KO, H.Y.: The Colorado Centrifuge Facility, *CENTRIFUGE 88*, 1988, pp.73-75.

44) TERASHI, M., ANDO, K., HOSOYA, S. and FUNASAKA, T.: Development of Uualitative Photo-instrumentation System by means of 70 mm Data Camera & Analyzer, Optical Systems Engineering III, *Proc. SPIE* 389, 1983, pp.62-74.

45) KITAZUME, M.: Influence of Loading Condition on Bearing Capacity and Deformation, *Proc. of International Symposium on Geotechnical Centrifuge Model Testing*, 1984, pp.149-151.

46) TERASHI, M. and KITAZUME, M.: Bearing Capacity of a Foundation on Top of High Mound Subjected to Eccentric and Inclined Load, *Report of the Port and Harbour Research Institute*, Vol.26, No.2, 1987, pp.3-24.

47) KOBAYASHI, M., TERASHI, M., TAKAHASHI, K., NAKAJIMA, K. and KOTANI, T.: A New Method for Calculating the Bearing Capacity of Rubble Mounds (in Japanese), *Report of the Port and Harbour Research Institute*, Vol.26, No.2, 1987, pp.371-411.

48) TERASHI, M. and KITAZUME, M.: Bearing Capacity of Foundations on Top Surface of Slopes, *Proc. of the 8th Asian Regional Conference on Soil Mechanics and Foundation Engineering*, Vol.1, 1987, pp.415-418.

49) KOBAYASHI, M., TERASHI, M. and TAKAHASHI, K.: Bearing Capacity of a Rubble Mound Supporting a Gravity Structure, *Report of the Port and Harbour Research Institute*, Vol.26, No.5, 1987, pp.215-252.

50) KITAZUME, M. and IKEDA, T.: Influence of Horizontal Restriction in Eccentric Loading Test, *SOILS & FOUNDATIONS*, Vol.33, No.3, 1993, pp.187-195 (in Japanese).

51) TERASHI, M. and KITAZUME, M.: Interference Effect on Bearing Capacity of Foundations on Sand, *Report of the Port and Harbour Research Institute*, Vol.26, No.2, 1987, pp.413-436 (in Japanese).

52) TERASHI, M., ENDOH, K. and KITAZUME, M.: Planning of Model Tests and Reliability of Test Results - Bearing Capacity of a Circular Foundation on Sand -, *Report of the Port and Harbour Research Institute*, Vol.28, No.3, 1989, pp.59-79 (in Japanese).

53) KITAZUME, M. ENDOH, T. and TERASHI, M.: Bearing Capacity of Shallow Foundation on Normally Consolidated Ground, *Report of the Port and Harbour Research Institute*, Vol.27, No.3, 1988, pp.185-203 (in Japanese).

54) TERASHI, M. and KITAZUME, M.: Behavior of a Fabric-reinforced Clay Ground under an Embankment, *CENTRIFUGE 88*, 1988, pp.243-252.

55) TERASHI, M. and KITAZUME, M.: Fabric-Reinforced Embankment on Soft Clay Ground, *Report of the Port and Harbour Research Institute*, Vol.28, No.2, 1989, pp.33-47 (in Japanese).

56) KANDA, K. and TERASHI, M.: Practical Formula for the Composite Ground Improved by Sand Compaction Pile Method, *Technical Note of the Port and Harbour Research Institute*, No.669, 1990, 52 p. (in Japanese).

57) TERASHI, M. and KITAZUME, M.: Bearing Capacity of Clay Ground Improved by Sand Compaction Piles of Low Replacement Area Ratio , *Report of the Port and Harbour Research Institute*, Vol.29, No.2, 1990, pp.119-148 (in Japanese).

58) TERASHI, M., KITAZUME, M. and MINAGAWA, S.: Bearing Capacity of Improved Ground by Sand Compaction Piles, Deep Foundation Improvements: Design, Construction, and Testing, *ASTM STP* 1089, *American Society for Testing and Materials*, 1990,

59) TERASHI, M., KITAZUME, M. and OKADA, H.: Applicability of the Practical Formula for Bearing Capacity of Clay Improved by SCP, *Proc. of the International Conference on Geotechnical Engineering for Coastal Development, Geo-Coast '91*, Vol.1, 1991, pp.405-410.

60) TERASHI,M., KITAZUME,M., OWAKI, T. and OKADA, H.: Stability of Clay Improved by Sand Compaction Pile Method, *Soil reinforcement: full scale experiments of the 80's*, 1993, pp.607-634.

61) KITAZUME, M. and MURAKAMI, K.: Behavior of Sheet Pile Walls in the Improved Ground by Sand Compaction Piles of Low Replacement Area Ratio, *Report of the Port and Harbour Research Institute*, Vol.32, No.2, 1993, pp.183-211 (in Japanese).

62) TERASHI, M., KITAZUME, M. and KAWABATA, K.: Centrifuge Modeling of a Laterally Loaded Pile, *Proc. of the 12th International Conference on Soil Mechanics and Foundation Engineering*, Vol.2, 1989, pp.991-994.

63) TERASHI, M. and KITAZUME, M.: Influence of a Slope on the Lateral Resistance of a Long Pile, *Report of the Port and Harbour Research Institute*, Vol.30, No.2, 1991, pp.327-348 (in Japanese).

64) TERASHI, M., KITAZUME, M., MARUYAMA, A. and YAMAMOTO, Y.: Lateral Resistance of a Long Pile in or near the Slope, *CENTRIFUGE 91*, 1991, pp.245-252.

65) KITAZUME, M. and MIYAJIMA, S.: Lateral Resistance of Long Pile in Soft Clay, *CENTRIFUGE 94*, 1994, pp.485-490.

66) KITAZUME, M., TERASHI, M. AIHARA, N. and KATAYAMA, T.: Applicability of Fabri-Packed Sand Drain for Extremely Soft Clay Ground, *Report of the Port and Harbour Research Institute*, Vol.32, No.1, 1993, pp.101-123 (in Japanese).

67) KITAZUME, M., TERASHI, M. and AIHARA, N.: Centrifuge Model Tests on the Consolidation Behavior of Soft Clay with Fabri-Packed Sand Drain, *The North American Regional Conference on geosynthetics*, Vol.1, 1993, pp.393-406.

68) KATAYAMA, T., HITACHI, S., KITAZUME, M. and AIHARA, N.: Centrifuge Model Tests on Soft Clay Improved by Fabri-Packed Sand Drain, *Proc. of the Japan*

Society of Civil Engineers, No.481/3-25, 1993, pp.107-115 (in Japanese).

69) KATAYAMA, T., YAHIRO, A., KITAZUME, M. and NAKANODO, H.: Analysis and Experimental Study on Fabri-Packed Sand-Drains' Stability in Tokyo International Airport Extension Project, *Proc. of the Japan Society of Civil Engineers*, No. 486/6-22, 1994, pp.19-25 (in Japanese).

70) KITAZUME, M., TERASHI, M. and KATAYAMA, T.: Centrifuge Model Tests on the Consolidation Behavior of Soft Clay Improved by Fabri-Packed Sand Drain, *The International Conference on Soft Soil Engineering*, 1993, pp.792-797.

71) TERASHI, M., TANAKA, H. and KITAZUME, M.: Extrusion Failure of Ground Improved by the Deep Mixing Method, *Proc. of the 7th Asian Regional Conference on Soil Mechanics and Foundation Engineering*, Vol.1, 1983, pp.313-318.

72) TERASHI, M., KITAZUME, M. and YAJIMA, M.: Interaction of Soil and Buried Rigid Structure, *Proc. of the 11th International Conference on Soil Mechanics and Foundation Engineering*, Vol.3, 1985, pp.1757-1760.

73) TERASHI, M., KITAZUME, M. and NAKAMURA, T.: External Forces Acting on a Stiff Soil Mass Improved by DMM, *Report of the Port and Harbour Research Institute*, Vol.27, No.2, 1988, pp.147-184 (in Japanese).

74) TERASHI, M., KITAZUME, M. and NAKAMURA, T.: Failure Mode of Treated Soil Mass by Deep Mixing Method, *Technical Note of the Port and Harbour Research Institute*, No.622, 1988, 18p. (in Japanese).

75) KITAZUME, M. and TERASHI, M.: Effect of Local Soil Improvement on the Behavior of Revetment, *Proc. of the International Conference on Geotechnical Engineering for Coastal Development, Geo-Coast '91*, Vol.1, 1991, pp.341-346.

76) KITAZUME, M., NAKAMURA, T. and TERASHI, M.: Reliability of Clay Ground Improved by the Group Column Type DMM with High Replacement, *Report of the Port and Harbour Research Institute*, Vol.30, No.2, 1991, pp.305-326 (in Japanese).

77) KITAZUME, M.: Model and Analytical Studies on Stability of Improved Ground by Deep Mixing Method, *Technical Note of the Port and Harbour Research Institute*, No.774, 1994, p.73 (in Japanese).

78) INATOMI, T., KAZAMA, M., IAI, S., KITAZUME, M. and TERASHI, M.: Development of an Earthquake Simulator for the PHRI Centrifug, *CENTRIFUGE 88*, 1988, pp.111-114.

79) De BEER: Bearing Capacity and Settlement of Shallow Foundations on Sand, *Proc. of a Symposium on Bearing Capacity and Settlemet of Foundations*, 1965, pp.45-33.

80) YAMAGUCHI, H., KIMURA, T. and FUJII, N.: On the Influence of Progressive Failure on the Bearing Capacity of Shallow Foundation in Dense Sand, *SOILS AND*

FOUNDATIONS, Vol.16, No.4, 1976, pp.11-22.

81) MERYERHOF, G.G.: The bearing Capacity of Foundations under Eccentric and Inclined Loads, *Proc. of the 3rd International Conference on Soil Mechanics and Foundation Engineering*, 1953, pp.440-445.

82) EASTWOOD, W.: The Bearing Capacity of Eccentrically Loaded Foundations on Sandy Soils, *Structural Engineer*, Vol.29, 1955, pp.181-187.

83) PRAKASH, S. and SARAN, S.: Bearing Capacity of Eccentrically Loaded Footings, *Proc. ASCE*, Vol.97, No.SM1, 1971, pp.95-117.

84) PURKAYASTHA, R.D. and CHAR, R.A.N.: Stability Analysis for Eccentrically Loaded Footings, *Proc. ASCE*, Vol.103, No.GT6, 1977, pp.647-651.

85) JUMIKIS, A.R.: Rupture Surfaces in Sand under Oblique Load, *Proc. ASCE*, Vol.8, No.SM1, 1956, pp.1-26.

86) DAVIS, E.H. and BOOKER, J.R.: The Effect of Increasing Strength with Depth on the Bearing Capacity of Clays, *Geotechnique*, Vol.23, No.4, 1973, pp.551-563.

87) VAUGHAN, P.R., CHAMRAWY, M.K., HAMZA, M.M. and HIGHT, D.W.: Stability Analysis of Large Gravity Structures, *BOSS '76*, 1976, pp.467-487.

88) YAGYUU, T. and YUKITA, Y.: Field Rupture Test of Soil Improved by Sand Compaction Piles with Low Sand-replacement Ratio, *Proc. of the 24th Japan National Conference on Soil Mechanics and Foundation Engineering*, 1989, pp.1891-1894 (in Japanese).

89) KUBO, K.: Experimental Study of the Behavior of Laterally Loaded Piles, *Proc. 6th International Conference on Soil Mechanics and Foundation Engineering*, Vol.2, 1965, pp.275-279.

90) Bureau of Ports and Harbours: Technical Standards for Port and Harbour Facilities in Japan, *Ministry of Transport*, 1980.

91) KATAYAMA, T.: Meeting the Challenge to the Very Soft Ground - The Tokyo International Airport Offshore Expansion Project, *Proc. of the International Conference on Geotechnical Engineering for Coastal Development, Geo-Coast '91*, Vol.2, 1991, pp.954-967.

92) KITAZUME, M., AIHARA, N. and TERASHI, M.: Consolidation Behavior of the Soft Ground with Fabri-Packed Sand Drain, *Proc. of the 27th Japan National Conference on Soil Mechanics and Foundation Engineering*, Vol.2, 1992, pp.2189-2192 (in Japanese).

93) ABOSHI, H., MIZUNO, Y. and KUWABARA, M.: Present State of Sand Compaction Pile in Japan, Deep Foundation Improvements: Design, Construction, and Testing, *ASTM STP 1089, ASTM*, 1991, pp. 32-46.

List of symbols

A : cross sectional area of the model foundation base
B : foundation width
C_0 : undrained shear strength at the ground surface
D_{10}: effective grain size
D_r : relative density
e : load eccentricity
E_γ : reduction ratio of bearing capacity in eccentric loading
H : horizontal load component
M : moment load component
n : stress concentration ratio
N_γ: bearing capacity factor
p : soil resistance
U_c : uniformity coefficient
V : vertical load component
δ_h : horizontal displacement
δ_v : vertical displacement
ϕ' : angle of internal friction

港湾技研資料　No.787

1994.12

編集兼発行人　運輸省港湾技術研究所

発　行　所　運輸省港湾技術研究所

印　刷　所　阿部写真印刷株式会社

Edited by the Port and Harbour Research Institute
Nagase, Yokosuka, Japan.